



**HAL**  
open science

## Automatic sequential rain sampling to study atmospheric particulate and dissolved wet deposition

Thomas Audoux, Benoit Laurent, Servanne Chevaillier, Anaïs Féron, Edouard Panguï, Franck Maisonneuve, Karine Desboeufs, Sylvain Triquet, Gael Noyalet, Olivier Lauret, et al.

### ► To cite this version:

Thomas Audoux, Benoit Laurent, Servanne Chevaillier, Anaïs Féron, Edouard Panguï, et al.. Automatic sequential rain sampling to study atmospheric particulate and dissolved wet deposition. *Atmospheric Environment*, 2023, 295, pp.119561. 10.1016/j.atmosenv.2022.119561 . hal-04067156

**HAL Id: hal-04067156**

**<https://hal.science/hal-04067156>**

Submitted on 13 Apr 2023

**HAL** is a multi-disciplinary open access archive for the deposit and dissemination of scientific research documents, whether they are published or not. The documents may come from teaching and research institutions in France or abroad, or from public or private research centers.

L'archive ouverte pluridisciplinaire **HAL**, est destinée au dépôt et à la diffusion de documents scientifiques de niveau recherche, publiés ou non, émanant des établissements d'enseignement et de recherche français ou étrangers, des laboratoires publics ou privés.

# Automatic sequential rain sampling to study atmospheric particulate and dissolved wet deposition

Thomas Audoux<sup>\*1</sup>, Benoit Laurent<sup>1</sup>, Servanne Chevaillier<sup>2</sup>, Anaïs Féron<sup>1</sup>, Edouard Pangui<sup>2</sup>, Franck Maisonneuve<sup>2</sup>, Karine Desboeufs<sup>1</sup>, Sylvain Triquet<sup>1</sup>, Gael Noyalet<sup>1</sup>, Olivier Lauret<sup>2,3</sup>, Florian Huet<sup>3</sup>

5 <sup>1</sup>Université Paris Cité and Univ Paris Est Creteil, CNRS, LISA, F-75013 Paris, France

<sup>2</sup>Univ Paris Est Creteil and Université Paris Cité, CNRS, LISA, F-94010 Créteil, France

<sup>3</sup>Univ Paris Est Creteil, CNRS, ENPC, Université Paris Cité, OSU-EFLUVE, F-94010 Créteil, France

*Correspondence to:* Thomas Audoux ([taudoux@lisa.ipsl.fr](mailto:taudoux@lisa.ipsl.fr))

## 10 **Abstract.**

Wet deposition is a key mechanism influencing lifetime of particles in the atmosphere. It allows the deposition of particles via two distinct processes, washout and rainout. Wet deposition of particles is highly variable in space and time depending both on atmospheric aerosol loads and precipitation. This variability can be observed from an event to another as well as within an event. Studying the chemical composition of wet deposition can help us to understand the origin of the aerosols as well as the way they are deposited. Indeed, depending on their intrinsic properties, aerosols have specific chemical signatures. Sequential rain sampling provides a means to monitor the chemical composition of wet deposition throughout a rain event, trace its origin, and discuss the relative contribution of rainout and washout during a single event. In order to address these issues, an automatic sequential rain sampler was specifically developed to collect the rain in consecutive fractions. The sampler has a large sampling area (1 m<sup>2</sup>) and an automatic distribution system allowing the sampling of wet deposition with high temporal resolution to document intra-event deposition variability and a sufficient volume to analyze the dissolved and particulate phases of the rain. Two rain events collected in July 2021 and February 2022 in an urban site in the surroundings of the Paris agglomeration were studied. Our results allowed us to quantify how the total mass concentration decreases with the precipitation amount during a rain event until reaching a constant level. By combining elemental and ionic analysis, the evolution of particulate and dissolved major and trace element concentrations is documented for these two rainfall events. The particulate phase shows a higher decreasing trend than the dissolved one. Major elements such as Fe, Si and Al are predominantly in the particulate phase while trace metals (TMs), like Mn and Zn, are shared in both dissolved and particulate phases. However, each element shows an increasing ratio of its dissolved to total (dissolved + particulate) fraction as rainfall progresses, especially for TM. The study of dissolved compounds (SO<sub>4</sub><sup>2-</sup>, NH<sub>4</sub><sup>+</sup> and NO<sub>3</sub><sup>-</sup>) confirms that concentrations are decreasing with rainfall depth but that the variations are influenced by changes in rainfall intensity. The rainout and washout relative contributions to wet deposition are discussed regarding the studied chemical species and the rain events.

## **Key Words**

Wet deposition; Rain sequential sampling; Atmospheric aerosol; Ionic composition; Trace and major elements; Dissolved and particulate phases; rainout and washout

## 35 **1 Introduction**

Wet deposition is a set of physico-chemical processes allowing the removal of atmospheric aerosol particles by hydrometeor precipitation. As a key mechanism influencing the lifetime of particles in the atmosphere, wet deposition is a major process to be considered in order to describe particles concentrations (Textor et al., 2006), and hence their different impacts on air quality and climate. Moreover, by removing particles from the atmosphere to land and ocean surfaces, wet deposition constitutes an important input of chemical species for marine and terrestrial ecosystems (e.g., Wright et al., 2018), as major nutrients nitrogen (N) and phosphorus (P) (Galloway et al., 2008; Van Wambeke et al., 2021). Atmospheric wet inputs of trace metals (TMs) carried by aerosols are also known to affect marine ecosystem functioning, by delivering both essential (as Fe, Zn and Co; Mackey et al., 2012) or potentially toxic TMs (as Cu, Pb and Cd; Jordi et al., 2012; Paytan et al., 2009) to the ocean surface. Observations around the world have shown a strong spatial variation in the mass and chemical fluxes of wet deposition (e.g., Vet et al., 2014; Keresztesi et al., 2019) and hence on their environmental impacts. Besides total mass fluxes, understanding the dissolved and particulate partition of chemical species in the wet deposition fluxes is key for understanding the mechanism which determines their biogeochemical effects. Indeed, dissolved phase of deposition can be used as a proxy of bioavailability (Jickells et al., 2016; Fan et al., 2006).

50 The wet deposition process removes particles from the atmosphere using two distinct processes, the rainout and the washout (Pruppacher and Klett, 1996). The rainout corresponds to the in-cloud scavenging where either the aerosols act as a condensation nucleus for the hydrometeors making up the cloud, or are captured by droplets, already formed, by impaction (Seinfeld and Pandis, 2016). The washout refers to the below-cloud scavenging and correspond to the capture of particles by raindrops as they fall via, for example, impaction, interception and brownian diffusion mechanisms (Slinn, 1977). Wet deposition is therefore simultaneously influenced by cloud life cycle, through rainout process, and by local scavenging of atmospheric aerosols through washout processes (e.g., Bertrand et al., 2008). This can lead to an efficient removal of aerosol particles from the atmosphere in remote areas far from the source regions (e.g., Bergametti et al., 1989; Keene et al., 2015; Zhao et al., 2003), as well as in polluted areas (e.g., Kulshrestha et al., 2009; Tang et al., 2005). The contribution of rainout and washout to total wet deposition varies from one event to another as well as within an event. The partition between these processes depends on the studied environment (rural, urban...) and thus **on** the presence of local emissions (Aikawa et al., 2014; Ge et al., 2016), on meteorological characteristics such as rainfall amount, intensity and types (Ge et al., 2021; Bertrand et al., 2008) and on the vertical distribution of aerosols in the air column as a function of their loads and sizes (Lim et al., 1991; Bertrand et al., 2008). Modeling studies estimate aerosols wet deposition fluxes either by using theoretical or empirical scavenging coefficients to calculate rainout and/or washout contributions (Zhang and Vet, 2006; Gong et al., 2011) or by using

65 the washout ratio empirical concept (Duce et al., 1991). The dissolved and particulate partition of chemical species is mainly based on the solubility concept, which is fixed as a function of aerosol origin (Richon et al., 2018). Currently, large uncertainties remain in the modeling of aerosol wet deposition due to a lack of constraints on scavenging processes and a poor prediction of precipitation rates (Croft et al., 2010; Ryu and Min, 2022; Yang et al., 2015). In order to improve our understanding and representation of wet deposition in models, an effort has to be done to provide more in-situ deposition  
70 measurements and to document its variability.

Wet deposition is usually studied at the event or weekly basis in order to monitor dissolved, particulate or total (dissolved + particulate) chemical composition and thus deposition fluxes over a long period (Castillo et al., 2017; Vincent et al., 2016). These measurements are needed to document the temporal variability of wet deposition. However, it has also been shown that  
75 wet deposition is not constant during a rain event (e.g., Jaffrezo and Colin, 1988). The high intra-event variability of wet deposition can be linked to the evolution of the origin of the deposited particles as well as changes in the rainfall characteristics or in washout and rainout processes. For this purpose, it is necessary to continuously monitor the chemical composition of dissolved and particulate aerosols in wet deposition during a rainfall event. Some online measurements have been used to monitor the pH, conductivity and dissolved inorganic ions (Ames et al., 1987; Laquer, 1990). However, to study the chemical  
80 composition evolution of both the dissolved and particulate concentrations, sequential sampling is the only method enabling the acquisition of successive rain fractions. It is of particular interest because of the dependence of wet deposition on the rainfall characteristics, such as its intensity, droplet sizes and distribution (e.g., González and Aristizábal, 2012), which also evolves during the event. For instance, several studies have highlighted the existence of the so-called dilution effect (e.g., Hicks and Shannon, 1979; Lindberg, 1982), i.e., the dependence of rain concentrations with the amount of precipitation.  
85 Therefore, sequential collection allows documenting the evolution of chemical compound concentrations during a single rain event. Sequential sampling has been of great interest to study the evolution of acid deposition and their neutralization during rainfall since the '80s (e.g., Seymour et al., 1978; Burch et al., 1996; Aikawa and Hiraki, 2009; Chatterjee et al., 2010). Therefore, most of the studies in the literature were focusing on major elements and ions in the dissolved phase and only a few have investigated the evolution of TMs during a rainfall (Ambe and Nishikawa, 1986a; Luo, 2001; Shimamura et al., 2006;  
90 Anil et al., 2017) or the relative distribution of particulate and dissolved phases to total rain concentrations (Ma, 2006; Kasahara et al., 1996).

Chemical composition of rainfall can change between the time of collection and the chemical analysis due to changes in the equilibrium between particulate and dissolved phases (e.g., Krupa, 2002). Therefore, rain is often filtered to enhance  
95 preservation until analysis, and particulate phase is not systematically analyzed. However, it is necessary to have a complete description of rainfall (particulate and dissolved fractions), in order to have a complete documentation of scavenging processes as well as of chemical composition of wet deposition (e.g., Ambe and Nishikawa, 1986b; Krupa, 2002). Furthermore, it is necessary to monitor the total composition, i.e., both the particulate and dissolved phases in order to determine the sources of

the pollutants, for example by using enrichment factors (e.g., Desboeufs et al., 2022). Indeed, even if some markers are largely  
100 in one phase or the other (e.g., Na, S in the dissolved; Al, Ti in the particulate), some elements such as K, P have a non-  
negligible share in both phases (e.g., Cheng et al., 2021).

The intra-event evolution of chemical composition of rain has been used to discuss the relative importance of the rainout and  
washout processes to total wet deposition (e.g., Aikawa and Hiraki, 2009; Báez et al., 1993; Celle-Jeanton et al., 2009; Ge et  
al., 2021). Indeed, one assumption used in the literature is that the first increments of the rain event are influenced by both  
105 rainout and washout while the last fractions could be attributed to the scavenging by rainout only (Aikawa and Hiraki, 2009;  
Desboeufs et al., 2010; Germer et al., 2007; Karşı et al., 2018; Xu et al., 2017). Washout and rainout contributions to wet  
deposition may also reflect local sources (washout) and long-range transport (rainout). In addition, chemical composition as  
well as its evolution can be used to identify the anthropogenic and natural sources of atmospheric compounds and their  
evolution during wet deposition events (Keene et al., 1986; Safai et al., 2004; Cao et al., 2009).

110

This study presents the development of an automatic sequential precipitation sampler in order to document the evolution of  
chemical composition both for the dissolved and particulate phases during the rainfall event. We focus on major elements  
( $\text{NO}_3^-$ ,  $\text{NH}_4^+$  and  $\text{SO}_4^{2-}$ ), source markers (Al, Si, Fe, Ti,  $\text{Na}^+$ ,  $\text{Cl}^-$ ) and TMs (Zn, Mn). From two rain events collected in an  
urban area close to Paris, we investigate the temporal dynamic of deposition during rain events, the origin and partition between  
115 dissolved and particulate phase of scavenged chemical species as well as the relative contribution of wet deposition processes  
(washout/rainout) in the total wet deposition.

## 2 Materials and Methods

### 2.1. Sampling site

The sampling of two rain events on 27 July 2021 (hereafter as R1) and 10 February 2022 (hereafter as R2) are done on the air  
120 quality **study site** operated by the Interuniversity Laboratory of Atmospheric Systems (LISA) and located at the University of  
Paris Est Creteil (UPEC) in the south-east of the Paris agglomeration (48.79°N-2.44°E). This study site is co-located with the  
OASIS atmospheric observatory (Chelin et al., 2015). It is an urban environment close to multiple sources of pollution such  
as local industries and an incinerator (1 – 2 km), multiple highways (0.1 – 0.5 km), railway stations (0.8 km), and civil  
construction sites.

125 Wet deposition collection is performed with a sequential sampler developed specifically for this study concomitantly with  
measurement of meteorological parameters with instrumentation on the air quality measurement site.

### 2.2 Sequential rain sampler

The design of sequential rain sampler has to satisfy several requirements. In order to precisely document the evolution of  
concentrations during a rain event and to better understand it, the collection must be performed at high temporal resolution

130 (from a few seconds for convective rain rates to tens of minutes for very low drizzle). Secondly, in order to investigate the evolution of scavenging processes during the rain event, it is necessary to have information throughout the event until its end. For this purpose, a large sampling area should allow collecting numerous rain fractions with a high temporal resolution during one event. In addition, the sampling line and the distribution unit have to allow the collection of several successive fractions without mixing them. Then, as our objective is to document the chemical composition for both the dissolved and particulate  
135 phase, the sampled rain volume needs to be at least equal to 50 mL to carry out a set of analyses. Moreover, TMs are expected to be present in very low concentrations at the end of the rain event. Therefore, it is critical to limit various chemical contamination for TMs measurements. Finally, it needs to be automated as much as possible so that it can be deployed in different environments and run with limited operator interventions.

A scheme of the sequential sampler developed at the LISA is presented in figure 1a. It is a 2 m high closed structure composed  
140 of a Teflon pyramid funnel with a collection surface of 1 m<sup>2</sup> that allows sampling rainwater into 24 successive fractions (adjustable from 0.05 to 0.5 mm) with a high temporal resolution controlled by volume. The pyramid funnel is closed up with a cover which is removed manually at the onset of each rain event in order to avoid dry deposition in the sampler and to collect the first raindrops. During the sampling, the rainwater collected in the pyramid funnel flows into a separating funnel made with Teflon and connected via a polypropylene (PP) connector. The rain sequential sampling is managed by an optical level  
145 sensor placed on the separating funnel (Fig. 1b). When a predefined range of rainwater volume is reached, the optical sensor triggers a peristaltic pump which empties the separating funnel (50 - 150 mL) into a sampling bottle in 4 s via the distribution unit. The distribution unit consists of two interlocking PP parts (Fig. 1c). The upper part is the rotating part of the unit (rotor) and has one port equipped with a PTFE connector for the transfer of rainwater from the peristaltic pump to the lower part of the distribution unit (stator). The latter has 24 holes with PTFE connectors for the distribution of rainwater to the sampling  
150 bottles through PTFE tubes. All tubes are connected to the sampling bottles through a cap specially designed allowing the flow of rainwater (into the rain inlet) while pushing out the air of the bottle throughout the air outlet on which is placed a syringe filter of pore size 0.2 µm to avoid atmospheric particle contamination. The change of sampling bottles is assured by a control unit that successively serves 24 PP bottles (Fig. 1b). The control unit can be programmed to set beforehand the volume of each sampling position and to collect the rainfall automatically (Fig. S1 in supplements). The system unit controls if the programmed  
155 volume in a sampling bottle is reached. When the latter is reached, the control unit note in a text file, the sampling line number, the date and hour and then triggers the stepper motor to rotate the rotor part by 15° to the next position. Once the rotation is complete, the collection bottle is closed by the rotor disc and rainwater cannot flow into it. The total volume of rainfall fractions collected sequentially can be up to 13 mm (+ field blank), the last position can be used for a larger volume collection of the end of the rain (2 mm of additional rainfall). The sampling device associated to the control unit allows us to adapt the collection  
160 of rain and be able to sample several fractions of very light to very intense rainfall (up to 60 – 70 mm h<sup>-1</sup>) with a minimum rainfall depth of 0.05 mm for each fraction without mixing.

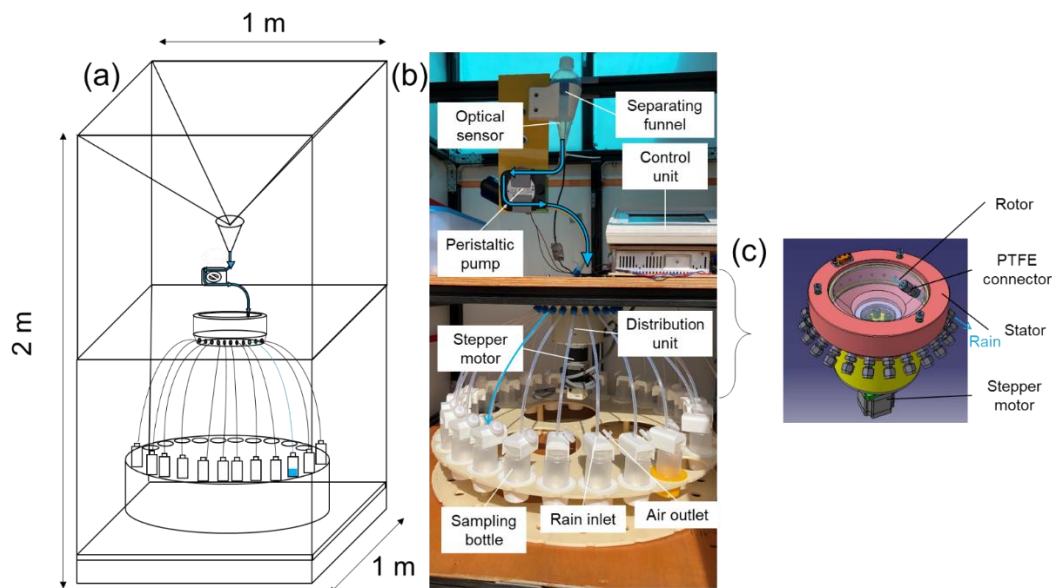


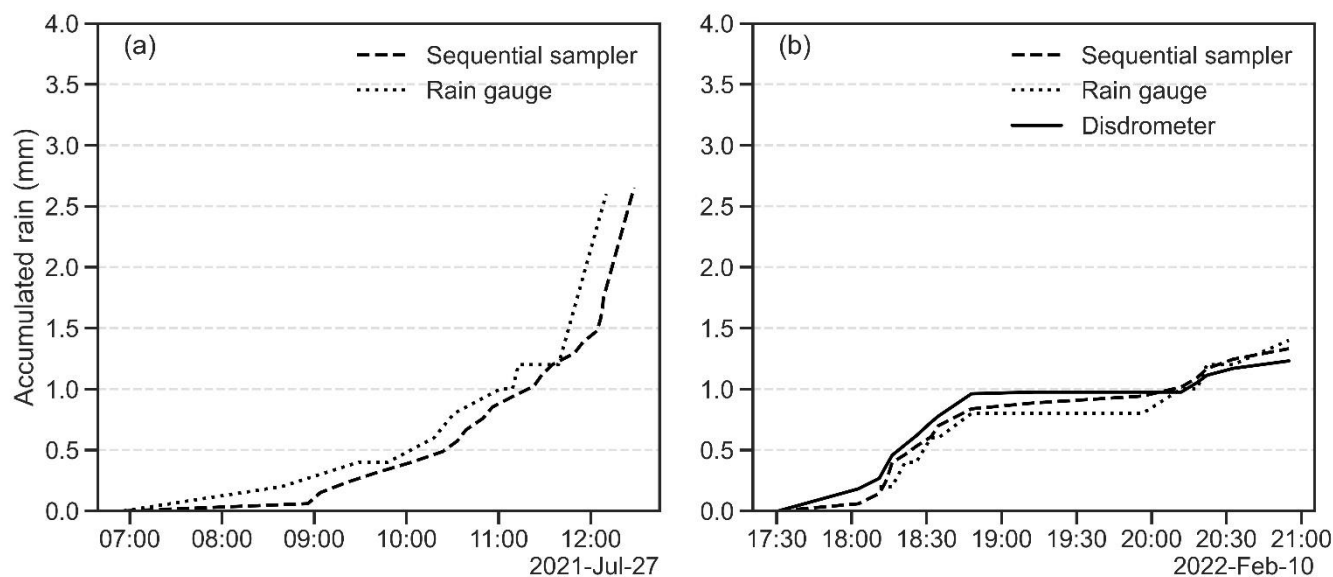
**Figure 1. (a) Scheme of the rain sampler, (b) overview of the distribution system and (c) scheme of the distribution unit. Blue lines represent the rainfall runoff.**

165

### 2.3 Meteorological conditions

In order to characterize atmospheric conditions associated to rain events, meteorological measurements were done in the air quality station of the LISA. Rainfall was monitored using a Précis-Mécanique rain gauge model 3070A (0.2 mm precision). In parallel, other parameters characterizing the air masses at the site have been measured such as air temperature, relative humidity using instrumentation from Campbell Scientific© and are recorded with a time step of 1 min.

Since February 2022, an optical disdrometer OTT PARSIVEL® (PARTicle SIZE and VELOCITY) has been deployed to monitor rainfall with 0.001 mm h<sup>-1</sup> precision. In order to qualify how the sequential sampler collects the rain fraction, we compared the accumulated rain collected by this device with rainfall measured by the rain gauge for the first rain collected on July 27, 2021 (R1, Fig. 2a) and rainfall measured by the rain gauge and the disdrometer for the second rain collected on February 10, 2022 (R2, Fig. 2b). The three devices show similar temporal evolution of the accumulated rainfall for R1 and R2. The sequential sampler is able to correctly collect rain fractions for low rain intensity as well as for intense rain registered by the rain gauge and the disdrometer.



180 **Figure 2. Accumulated rain collected and measured as a function of time for two rain events (a) R1 event in July, (b) R2 event in February.**

In a complement to local wind measurements performed at the studied site, air masses' trajectories were computed using the HYSPLIT model (<http://ready.arl.noaa.gov/HYSPLIT.php>) (Draxler and Rolph, 2003). HYSPLIT forward and backward air mass simulations can be respectively used to study local to continental air mass dispersion and transport of atmospheric compounds (e.g., Celle-Jeanton et al., 2009; Bertrand et al., 2008; Calvo et al., 2012) and to identify the origin of air masses in order to identify sources of atmospheric substances, e.g., mineral dust, sea salt or anthropogenic (e.g., Vincent et al., 2016; Anil et al., 2017). Here, 48h backwards trajectories were computed by the HYSPLIT model, with GFS (0.25°, global), from the studied site (47.79°N – 2.44°W) at 0 m, 500 m and 1 000 m a.g.l. in order to have information about the origin of the air mass scavenged on the first kilometer of the atmospheric column for R1 on July 27, 2021, 06:00 and 12:00 GMT and R2 on February 10, 2022, 18:00 and 20:00 GMT.

## 2.4 Analytical and sampling protocols

The dissolved and particulate concentrations in the rainwater can vary over several orders of magnitude from hundreds of ppm to few ppb to tens of ppt according to the element (e.g., Lim et al., 1991; Ma, 2006). In order to quantify low concentration, especially for TMs, the chemical contamination along the sequential sampling line of the sampler needs to be limited and controlled. Following Laquer (1990) recommendation, surfaces materials in contact with rainwater (i.e., collection's and storage's surfaces) have to be chosen based on the chemical compound to be analyzed. In our case, the interest elements are metals and inorganic ions, so the device is made with Teflon, PP and Neoprene® (peristaltic pump tube), which are metal-free material (Method 1638, 1996). Sampling bottles and all contact surfaces underwent a drastic washing protocol. The latter

200 consisted in washing, several soaking (24h in Decon© 2% v/v, 24h in HCl 0.4M Normapur® then 7 days in HCl 0.4M Suprapur®, 24h then 7 days in ultrapure water (UPW, 18.2 MΩ.cm)) and repeated rinses with reverse osmosis-purified and ultrapure waters (UPW) in ISO 7 then ISO 5-controlled laboratory rooms, respectively.

Samples are pretreated and conditioned for ionic and elemental analysis as presented in figure 3 after the end of rainfall within 1 to 12 hours. Otherwise, they are kept in the dark at  $T = 6^{\circ}\text{C}$ , and treated within 24 hours. The treatment, filtration and  
205 conditioning of the samples is carried out in an ISO 6-controlled laboratory room under a laminar flow hood (U15 filter) estimated ISO 3. For each sequential sample, pH measurements are done in a 5-10 mL aliquot using a pH meter (METTLER TOLEDO® Seven2Go).

The rest of the sample (60 to 145 mL depending on the collected fractions) is filtered through pre-cleaned Nuclepore® polycarbonate membranes with a porosity of  $0.2\ \mu\text{m}$  to separate the particulate phase from the dissolved phase. The filters are  
210 then dried under laminar flow hood then conditioned for 48h at a relative humidity of 45 – 50% and at a temperature between 20 and  $25^{\circ}\text{C}$  prior to weighing using a precision microbalance (METTLER TOLEDO® XPR26C, PRAMMICS Platform). Filtration is done from the last rain fractions to the first one in order not to risk any contamination of the less concentrated rainwater by the most polluted. Several rain sequential samples can be filtered on the same filter in order to accumulate sufficient material to obtain a mass on the filter with a confidence level of 95%. On the contrary, when particulate load is too  
215 high, one rain fraction is filtered on several membranes. Uncertainties are calculated according to the propagation of the weighing uncertainty of the filters with a confidence level of 95%. Elemental composition (Al, Ba, Ca, Cr, Fe, K, Mg, Mn, Na, Ni, P, S, Si, Ti and Zn) of successive particulate fractions is obtained using X-ray fluorescence spectrometer (XRF, ZETIUM 4 kW, MalvernPanalytical®, PRAMMICS Platform). For dissolved phase, all the sequential samples are analyzed even if there are more fractions describing dissolved than particulate phases. Ten milliliters aliquot of the dissolved phase is  
220 frozen until analysis of water-soluble major cations ( $\text{Na}^+$ ,  $\text{NH}_4^+$ ,  $\text{K}^+$ ,  $\text{Mg}^{2+}$ ,  $\text{Ca}^{2+}$ ) and anions ( $\text{Cl}^-$ ,  $\text{NO}_3^-$ ,  $\text{PO}_4^{3-}$ ,  $\text{SO}_4^{2-}$ ) by Ion Chromatography (Compact IC Flex, Metrohm®, PRAMMICS Platform). Organic ions ( $\text{HCOO}^-$ ,  $\text{CH}_3\text{COO}^-$ ,  $\text{C}_2\text{H}_5\text{COO}^-$ , MSA,  $\text{C}_2\text{O}_2^-$ ) can also be measured, but are not presented here. Two 15 mL aliquots are acidified to  $\text{pH} = 1$  with nitric acid (Suprapur®) and stored at  $7^{\circ}\text{C}$  protected from air and light until analysis by Inductively Coupled Plasma Atomic Emission Spectrometer (ICP-AES, Spectro ARCOS Ametek®) of water-soluble Al, Ba, Ca, Cr, Fe, K, Mg, Mn, Na, Ni, P, S, Si, Ti and  
225 Zn.

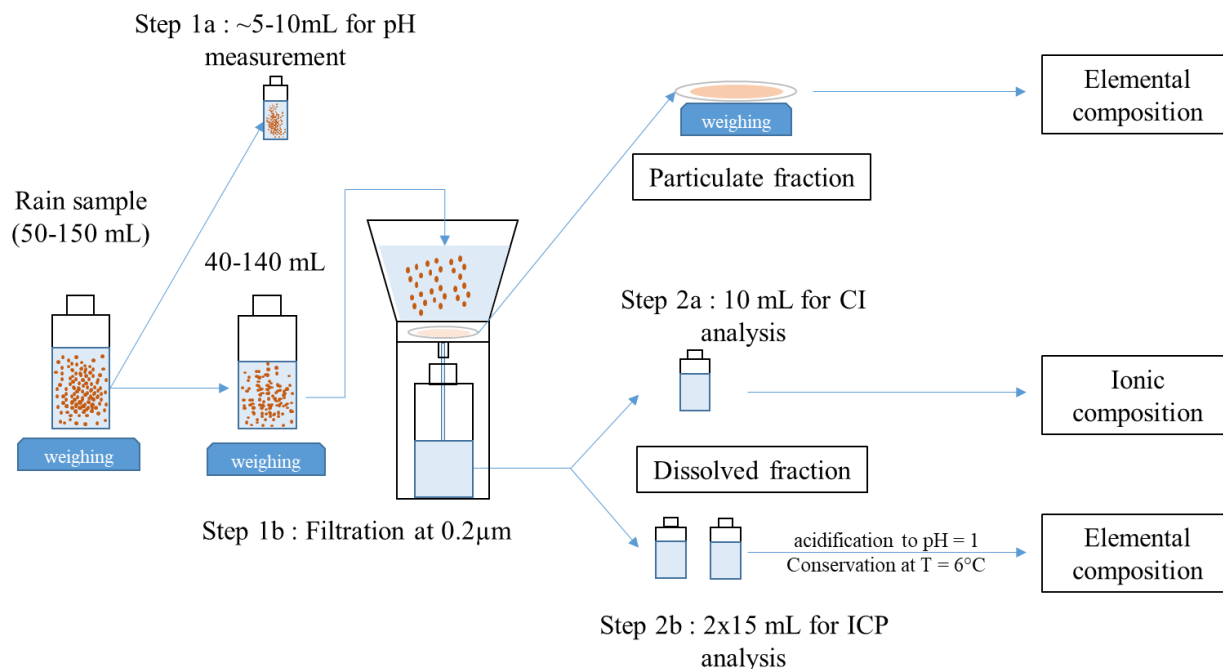


**Figure 3. Scheme of sample treatment and chemical analysis followed for each of the rain samples collected during a rain event.**

230 For XRF and ICP analysis, limits of detection (DL) are calculated as three times the standard deviation of laboratory analytical blanks, blank filters and acidified UPW, respectively (see table S2 in supplements). Uncertainties are defined as the standard deviation of analytical replicates. For IC, the quantification limit (QL) is determined empirically by comparing controls performed during the analysis and the calibration range. We assume the highest concentration for which there is a 10% difference with the calibration range is the QL. Then, DL is calculated as being equal to one third of the QL (see table S3 in

235 supplements). Uncertainties are defined as the relative deviation of controls with calibration range. The detection limits allow us to determine the expected dissolved concentrations at the end of the rain with detection limits ranging from few ppb (for nutrients and major element) to several tens of ppt (TMs).

Based on preliminary tests for optimizing rinse (see text S4 in supplement), the funnel is rinsed using 500 mL UPW prior to the collection of rain. Field blanks are done by pouring UPW over the funnel after the rinsing of the collection system, before

240 the onset of rainfall. The field blank values, if not below DL, represent in average less than 16.9 ppb (0.03 – 69.9ppb) compared to values obtained in the first 0.06 mm of rainfall up to 8 699 ppb for R1 and less than 41.2 ppb (0.1 – 358 ppb) compared to values obtained in the first 0.06 mm of rainfall up to 2 893 ppb for R2. However, the values obtained for the field blanks cannot be subtracted from each fraction as the successive fractions are not influenced the same way by initial sampling conditions.

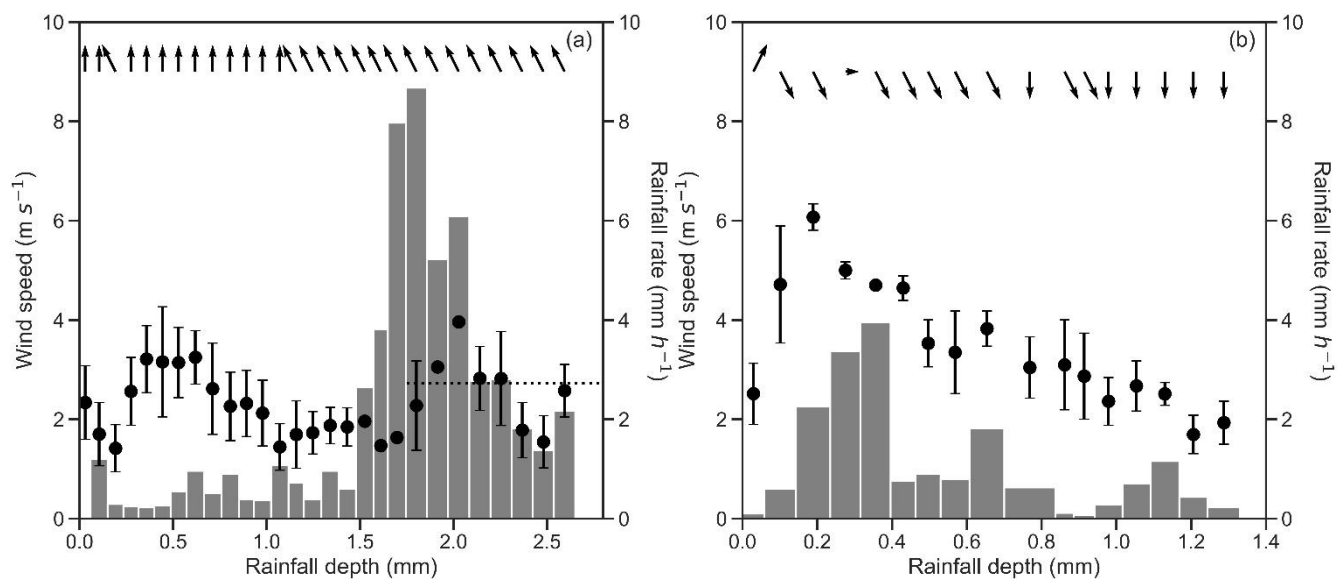
### 3 Results and discussion

#### 245 3.1 Rain sequential sampling conditions

The R1 was collected from 06:55 GMT until 12:25 GMT on July 27, 2021, i.e., for 5 hours 30 min. The total rainfall was 2.65 mm, collected in 20 fractions between 0.06 and 0.1 mm, plus a last one being of 0.91 mm to collect the end of rain (Fig. 4a). The R2 was collected from 17:28 GMT until 20:55 GMT on February 10, 2022, i.e., for 3 hours 27 min, in 17 fractions between 0.05 and 0.14 mm for a total rainfall depth of 1.33 mm (Fig. 4b).

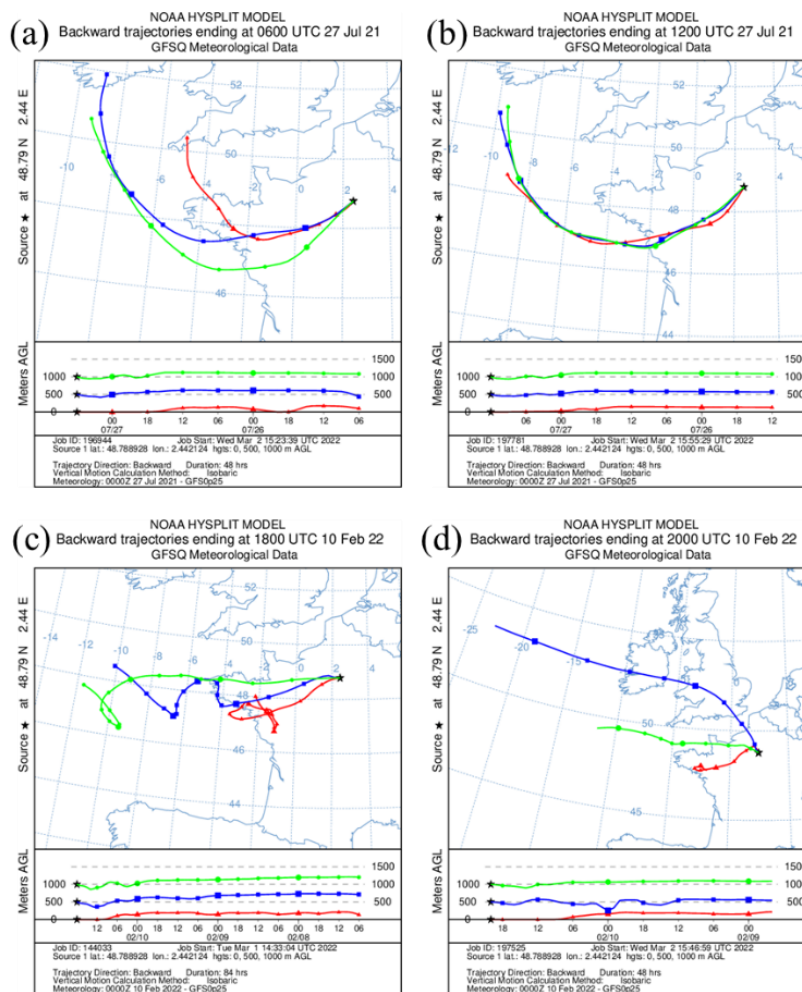
250 R1 wind speeds ranged from 0.5 to 5.0 m s<sup>-1</sup> (average = 2.4 ± 0.9 m s<sup>-1</sup>) and were coming from south all along the event. Wind speeds during R2 were higher than during R1, ranging from 1.1 to 6.5 m s<sup>-1</sup> (average = 2.9 ± 1.1 m s<sup>-1</sup>) and coming from west-south-west for the first collected fraction then north-north-west for the rest of sequential samples. On the contrary, the temporal dynamics of the rain pattern were very contrasted both during R1 and R2. For R1, rainfall intensity changed during the rain from 0.03 to 8.68 mm h<sup>-1</sup>. For R2, intensity ranged from 0.03 to 2.25 mm h<sup>-1</sup>. As sequential collection is based on volume, this  
255 illustrates the wide variation in collection time for each fraction (from 43s to 2 h).

R1 as well as R2 can be separated into four rainfall phases, based on rainfall regime (Fig. 4). Phase I of R1, between 0.06 – 0.49 mm, is characterized by a decreasing rainfall rate to 0.22 mm h<sup>-1</sup>. Phase II, between 0.49 – 1.48 mm, is characterized a steady rainfall rate of 0.68 ± 0.26 mm h<sup>-1</sup>, when the phase III, between 1.48 – 1.85 mm, is characterized by an increase of rainfall rates up to 8.68 mm h<sup>-1</sup> to finally decrease until the end of the event (phase IV). For R2, the phase I, between 0.00 –  
260 0.40 mm, is characterized by an increasing rainfall rate from 0.10 to 3.95 mm h<sup>-1</sup>. Phase II, between 0.40 – 0.61 mm, is characterized by constant rainfall rate of 0.82 ± 0.07 mm h<sup>-1</sup> and the phase III, between 0.61 – 0.94 mm, is characterized by a decreasing rainfall rate from 1.82 to 0.08 mm h<sup>-1</sup>. The last phase IV presents a Gaussian distribution of rainfall rates with a maximum of 0.9 mm h<sup>-1</sup> around 1.17 mm. Based on the HYSPLIT 48h backwards trajectory calculation (Fig. 5), the origin of air masses scavenged by rain events were homogeneous on the precipitation period and came from the Atlantic Ocean for R1  
265 and R2 events. Both local winds and the origin of air masses transporting aerosols were stable throughout both events.



270

**Figure 4.** Evolution of mean wind speed (black dot, median wind direction (black arrows) and of rainfall rates (grey bar plot) as a function of rainfall depth during each sample of R1 (a) and R2 (b). The black dotted line corresponds to the mean rainfall rate of the last fraction of R1 during 1.75 – 2.65 mm (a). The tip of the arrow pointing in the direction (North upward and South down), while uncertainty bars correspond to standard deviation of wind speed during rain fractions' collection time. To give an example of how to read the figure, when the tip of the arrow is heading upwards, it means that the wind is coming from the south.



275 **Figure 5. 48 h Air mass backward trajectory arriving at Creteil, France, for R1 (a and b) and of R2 events (b and c) for air masses reaching 0 m, 500 m and 1000 m of altitude at the beginning (a et c) and the end (b and d) of rain events**

### 3.2 Intra-event variability of wet deposition

#### 3.2.1 Total mass concentrations and chemical contributions

Particulate and dissolved mass concentrations as well as chemical contributions are represented as a function of rainfall depth  
 280 for both R1 and R2 events (Fig. 6). The chemical composition of the two wet deposition events, described from the minimum, maximum and volume-weighted mean (VWM) values, is available in the supplement table S5. The 20 and 15 fractions of rain samples collected for R1 and R2 have been filtered on 8 and 5 filters, respectively. The mass concentrations of each rain fractions are obtained with a confidence level of 95% by weighting filters with the exception of the fraction 0.67 – 1.29 mm on the filter of R1. Therefore, no particulate mass concentration information between 0.67 and 1.29 mm of precipitation amount  
 285 is presented.

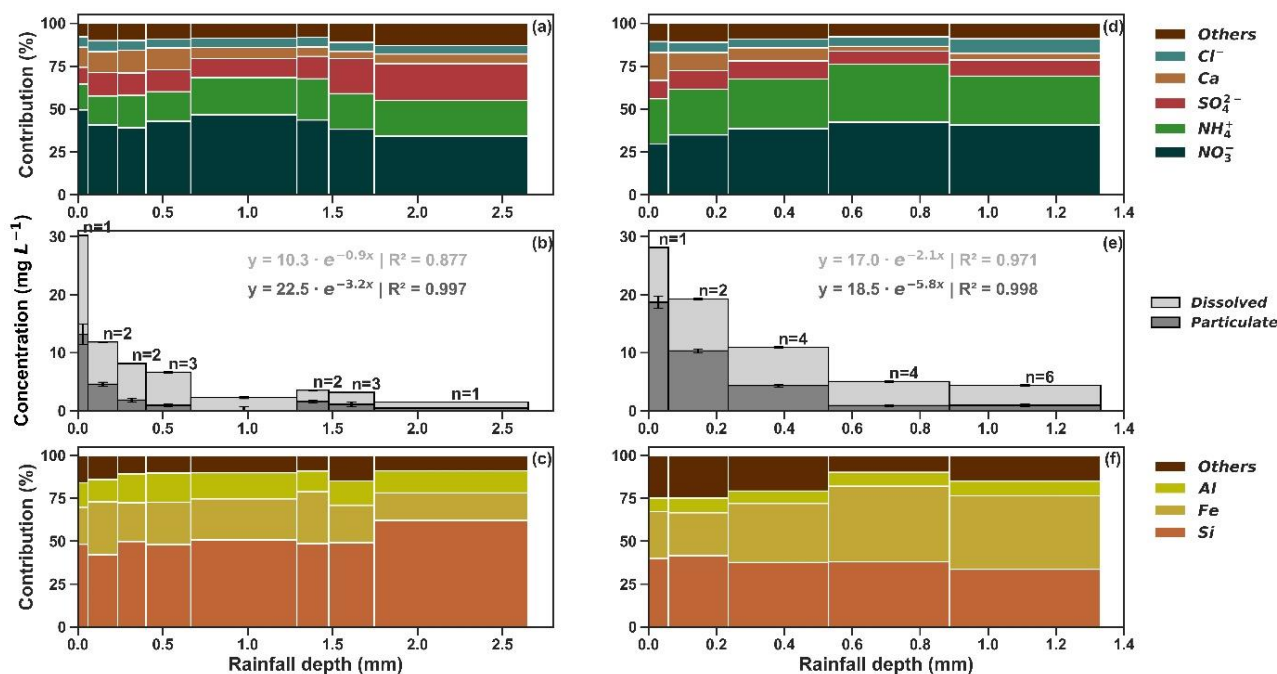


Figure 6. Evolution of total mass rain concentrations (in mg L<sup>-1</sup>) for R1 (b) and R2 (e) and contributions (in %) of dissolved compounds (a and d) and particulate elements (c and f) with rainfall depth (mm). It must be noted that dissolved concentrations do not take into account organic carbon. Uncertainty bars are presented for dissolved and particulate phases. The number of fractions cumulated on each filter is noted next to each bar.

290

295

300

305

Figure 6 emphasizes firstly that total mass concentrations decrease quickly with rainfall depth for both R1 and R2 until reaching constant values (Fig 6 b and e). The first sequential samples of R1 and R2 account for 14 to 16% of total mass fluxes while being responsible for only 2 to 4% (0.06 mm of rainfall depth) of the total rainfall amount of each event (Fig. 6 b-e). It must be noted that the particulate mass concentration increases for R1 between the 0.40 – 0.67 mm and the 1.29 – 1.48 mm rain fractions concomitantly with the increase of rainfall rates observed in figure 4b. For both events, the decreasing trend of the particulate phase concentration is more pronounced than the dissolved one. Indeed, 59 – 60% of the particulate and 30 – 41% of the dissolved mass fluxes occur during the first 15 – 18% of accumulated precipitation. In the literature, concentrations of particulate phases have been shown to follow a higher decreasing trend with precipitation amount than dissolved phase. This indicates that particulate components are more easily scavenged by raindrops (Kasahara et al., 1996; Ma, 2006).

In order to explore the decreasing pattern, we plotted an exponential fit ( $y = a \cdot e^{-bx}$ ) of dissolved as well as particulate mass concentrations as a function of rainfall depth, y being the concentrations, x the rainfall depth and b the exponential decay parameter. Exponential fit parameters for dissolved and particulate phases evolution of both R1 and R2 events are shown on Figure 6 and described in the table 1. The decay of the particulate phase concentrations with rainfall depth is between 2.4 and 2.8 times greater than those of the dissolved phase. These equations support the fact that higher scavenging is observed at the beginning of rain events, with a most marked decreasing trend for the particulate phase.

**Table 1. Exponential parameters of the dissolved and particulate mass concentrations evolution of R1 and R2**

Event	Dissolved phase		Particulate phase	
	R1	$y = 10.3 \cdot e^{-0.9x}$	$R^2 = 0.877$	$y = 22.5 \cdot e^{-3.2x}$
R2	$y = 17.0 \cdot e^{-2.1x}$	$R^2 = 0.971$	$y = 18.5 \cdot e^{-5.8x}$	$R^2 = 0.998$

310 Figure 6 also emphasizes that the relative contribution of the different compounds in the dissolved and particulate phases is fairly similar in the two events. The stability of chemical contribution is consistent with the homogeneity of local wind direction and back trajectories (see 3.1.) during the rain events. Therefore, one can assume that the transported and scavenged air masses present a certain continuity throughout both rainfall events. Dissolved composition of rainwater is dominated by sulfate, nitrate and ammonium for both rain events. Their cumulated contribution is 74% for R1 and 79% for R2 of dissolved mass concentration measured in average (Figure 6a-c for R1 and figure 6d-f for R2). Even though air masses originate from the Atlantic Ocean, the influence of sea salt at the receptor site is low considering the low contribution of chloride and sodium in rain composition for both rainfalls (less than 7% for Cl in rain sequential samples). Thus, rain event composition seems to be mainly influenced by the scavenging of anthropogenic secondary inorganic aerosols such as ammonium nitrate and ammonium sulfate, or their gaseous precursors, NO<sub>x</sub>, NH<sub>3</sub> or SO<sub>2</sub>. Indeed, these compounds are resulting from the conversion of compounds related to anthropogenic activities such as fossil fuel emissions (conversion of NO<sub>x</sub> into NO<sub>3</sub><sup>-</sup> and SO<sub>2</sub> into SO<sub>4</sub><sup>2-</sup>) and agricultural emissions (NH<sub>3</sub> into NH<sub>4</sub><sup>+</sup>) and are mainly in the submicron particulate matter (PM<sub>1</sub>). NH<sub>4</sub><sup>+</sup> and NO<sub>3</sub><sup>-</sup> VWM concentrations are 2.7 and 1.6 times higher for R2 than R1, respectively. Higher NH<sub>4</sub><sup>+</sup> content could be attributed to higher urban emissions of NH<sub>3</sub> and to early nitrogen fertilizer applications in February (Airparif, 2021; Favez et al., 2021). Higher NO<sub>3</sub><sup>-</sup> content can be due to lower winter temperatures that facilitate the formation of particulate nitrate (e.g., Cao et al., 2017; Schaap et al., 2004). The higher pH found in R2 (6.1 – 6.8) in comparison to R1 (4.9 – 6.1) (see supplement table S5) is in agreement with a pH neutralizing effect due to ammonium, previously observed in Paris (Beysens et al., 2017), which concentrations are inferior in R1 samples. Ammonium sulfate and ammonium nitrate aerosols are composed of mineral salts and are therefore highly soluble. Thus, dissolved concentrations are generally considered to represent total concentrations. The comparison between total S and SO<sub>4</sub><sup>2-</sup> concentrations show that 94 to 97% of S is under sulfate form depending on the rainfall event, confirming that assumption.

330 Particulate phase is composed in the majority of Si, Fe and Al, representing more than 75% of the total elements that have been analyzed, whatever the rain sequential samples. The presence of construction sites (Si, Al) and highways (Fe) close to the receptor site may explain the high contribution observed for these elements, since these elements, as also Zn, Ba and Ti are known to be related with non-exhaust traffic emission as tire and brake wear or resuspended particles (e.g., Thorpe and Harrison, 2008; Pant and Harrison, 2013). Typically, these elements are associated with the mode of PM higher than 2.5 μm

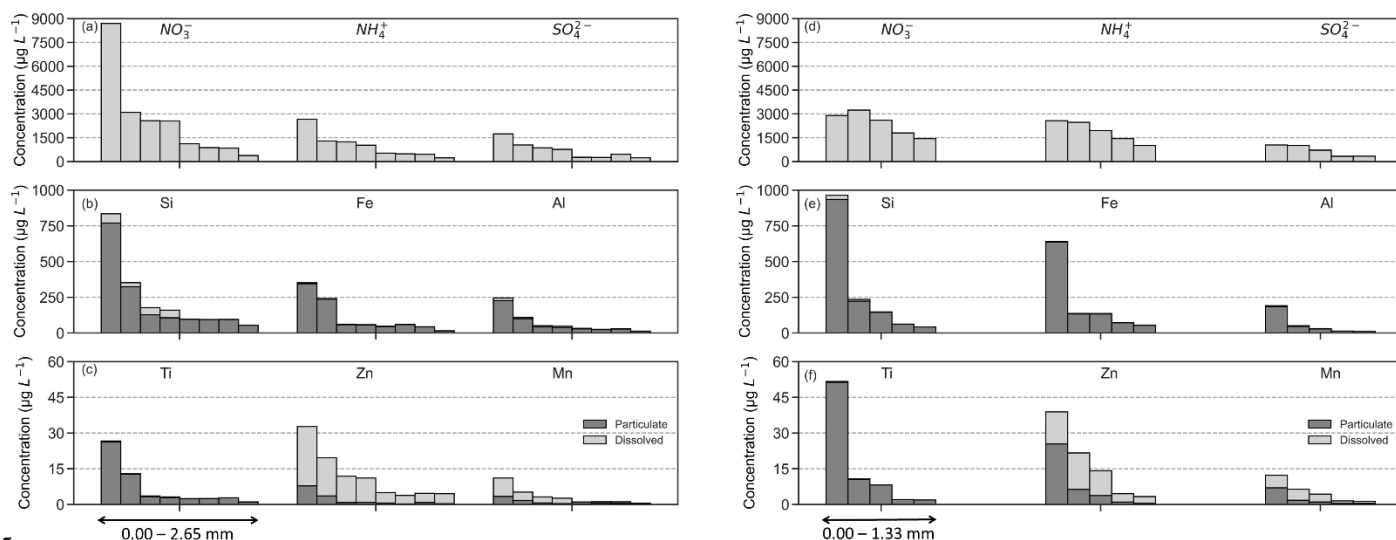
(Bukowiecki et al., 2009; Mamun et al., 2020). It is also interesting to note that Fe, Si, Al and Ti are predominantly found in the particulate phase of both rain events (see supplements table S5).

Among TMs, Ti is predominantly in the particulate phase whereas Zn and Mn are present in both the dissolved and particulate phase (these elements are part of ‘others’ class in fig. 6). Their contribution in the mass concentrations of each fraction, depending on the rain event, are ranging from 0.02 to 0.06% and for Mn and from 0.08 to 0.40% for Zn in the dissolved phase and from 0.10 to 0.39% for Mn, from 0.13 to 1.2% for Zn and from 1.2 to 2.2% for Ti, respectively in the particulate phase. Ti is mainly of crustal origin while Mn and Zn have various sources in the urban environment such as exhaust and non-exhaust emissions from road traffic, construction sites and incineration plants (e.g., Pant and Harrison, 2013; Sanderson et al., 2014; Citepa, 2022). However, due to the continuity of scavenged air masses, we estimate that their origins are stable all along the rainfall.

### 3.2.2. Chemical concentration evolution

#### *Evolution with rainfall depth*

The evolution of chemical concentrations is detailed in the figure 7 for major chemical species and TMs composing the rains. As it has been observed for mass concentrations, the major chemical species and TMs concentrations decrease quickly between the first sample and the next ones. Even if the general trend is a decrease of mass and chemical concentrations with rainfall depth, the decreasing patterns are both different from one rain to another but also from a chemical species to another. The final chemical concentrations are between 8 and 24 and between 2 and 27 times smaller than the values measured at the beginning of the rainfall R1 and R2, respectively.



355

**Figure 7. Evolution of concentrations of dissolved and particulate species in rainwater for R1 (a, b, c) and R2 (d, e, f) with rainfall depth. The dark gray area and light gray correspond to the particulate and dissolved phases, respectively. Each R1 bar corresponds to the fractions 0.00 – 0.06 mm, 0.06 – 0.23 mm, 0.23 – 0.40 mm, 0.40 – 0.67 mm, 0.67 – 1.29 mm, 1.29 – 1.48 mm, 1.48**

360 – 1.75 mm and 1.75 – 2.65 mm, respectively. Each R2 bar corresponds to the fractions 0.00 – 0.06 mm, 0.06 – 0.23 mm, 0.23 – 0.53 mm, 0.53 – 0.89 mm and 0.89 – 1.33 mm, respectively.

Figure 7 highlights a difference of scavenging of dissolved and particulate phases. The concentrations of elements mainly present in the particulate phase follow the same marked decreasing trend during the rain for both R1 and R2 (Al, Si, Fe and Ti in Fig. 7b and 7e). The general pattern for the concentrations evolution of soluble species differs between the two rains with  
365 lower decrease observed for R2 (nitrate, ammonium and sulfate in Fig. 7a and 7d). Al, Si and Fe (which account for 73 to 90% of elemental composition of the particulate phase) are generally associated with PM higher than 2.5  $\mu\text{m}$  (Bukowiecki et al., 2009; Mamun et al., 2020), while sulfate, nitrate and ammonium (depicting altogether for 69 to 86% of the dissolved phase mass according to rain events or fractions) are associated mainly with PM<sub>1</sub> fraction. The difference observed for the decays could be explained by the difference in particle sizes. Indeed, washout is a particle size-dependent process which shows a  
370 minimum in the diameter range 0.2 - 2  $\mu\text{m}$  (the so-called Greenfield Gap; Greenfield, 1957). Therefore, the largest particles (here Al, Si, Fe) are more easily removed and thus represent a larger fraction of the deposited particles at the beginning of the rainfall and a lowered proportion as the rainfall progresses, as also described by Karşı et al. (2018). The latter imply this overwhelming presence of smaller particles at the end of the rainfall event to a lower efficiency of the washout process to scavenge this range of particles, and a higher relative contribution of the rainout process in wet deposition.

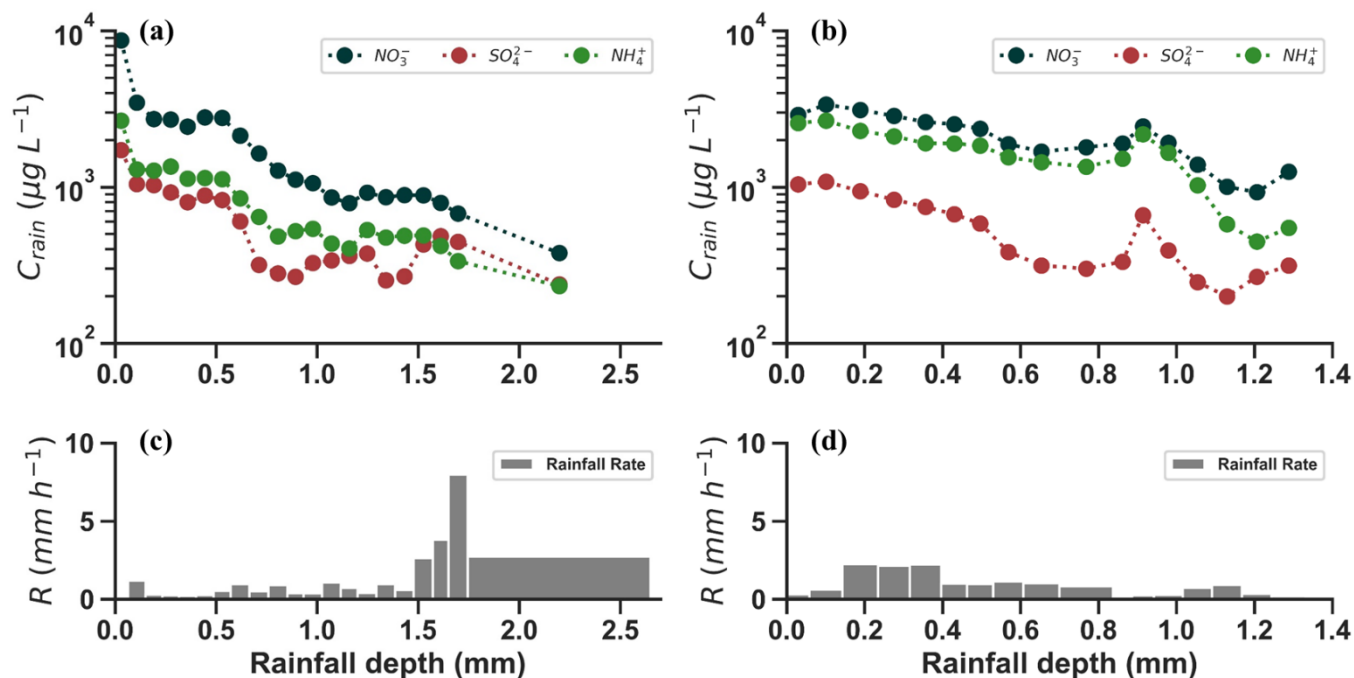
375 Figure 7 also illustrates that dissolved/total ratio of elements increases between the first and the last collected fractions. This ratio could be related to fractional solubility (hereafter referred as solubility) commonly used to understand dissolution processes. As an example, solubility increases during rainfalls for Mn (from 50 to 86% in R1 and from 43 to 62% in R2), Zn (from 76 to 93% in R1 and from 35 to 86% in R2) and Fe (from 2.1 to 10% for R1 and from 0.7 to 2.0% in R2).

Our results are consistent with a highest wet deposition at the beginning of the event due to the greater presence of particles in  
380 the atmospheric column under the cloud. At the later stage of a rain event, the atmospheric column is depleted of aerosols, then, the wet deposition flux is limited and thereby causes a decrease in the observed average rain mass and chemical concentration of the event. As mentioned in the introduction, the mass and chemical concentrations patterns found in R1 and R2 could be related with evolution from first samples affected by both rainout and washout, whereas last samples correspond predominantly to scavenging by rainout (Aikawa and Hiraki, 2009; Desboeufs et al., 2010; Germer et al., 2007; Karşı et al.,  
385 2018; Xu et al., 2017; Berberler et al., 2022). Our results support thus the fact that particulate phase, being deposited predominantly in the earlier stage of rain, is more likely to be scavenged by washout than rainout process.

### ***Evolution with rainfall rate***

Figure 8 illustrates the impact of changing rainfall regime on the sulfate, nitrate and ammonium (SNA) concentrations in the  
390 rainwater with a higher time resolution than total concentrations. Evolution of SNA concentrations observed for R1 (Fig. 8a) is consistent with the evolution of total concentrations described figures 6 b and 7. However, for R2 (Fig. 8b), SNA concentrations show a decreasing trend at the beginning of the event (0.00 – 0.84 mm). This is followed by an increase in

concentrations when the rainfall rate is minimum (last moments of phase III, sect. 3.1). Then, as the rainfall rate increases, the decreasing trend is re-established until the rainfall rate decrease again.



395

**Figure 8. Evolution of sulfate, nitrate and ammonium (SNA) concentrations for (a) R1 and (b) R2; evolution of rainfall rate for R1 (c) and R2 (d) with rainfall depth (mm).**

Disdrometer measurements (Fig. S6 in supplements) show an increase of the relative weight of smaller droplets concomitant with the increase of SNA concentrations observed between 0.8 and 0.9 mm (fig. 8b). On this basis, one can think that increases in SNA concentrations in rainwater during R2 may result from an increase in the scavenging efficiency, due to the smaller size of the rain droplets (Asman, 1980), or from an increase in droplet evaporation during their fall, leading to an increase in their concentrations (Huff and Stout, 1964; Baechmann et al., 1996a, b). In relation to this last hypothesis, we observed a decrease in surface relative humidity measured at our site. Additional ceilometer measurement made in Paris region (Haefelin et al., 2005) highlights the attenuation of the backscattered signal during the same time frame (Fig. S7 in supplements), which is consistent with a decrease of rainfall reaching the surface and hence evaporation of droplets.

405

### 3.3. Rainout and washout deposition contributions

As mentioned, the patterns of mass and chemical concentrations are consistent with evolution from the combined rainout and washout process in the first samples, then a scavenging mainly due to rainout. However, the contribution of these processes seems to be different for a chemical species to another (e.g., Aikawa et al., 2014). In order to deconvolute the contribution of each process for each chemical species, we used here the set of dissolved samples for soluble species, which have a higher

410

temporal resolution throughout both rainfall events than particulate samples (Fig. 8). We considered the total concentration (Fig. 9) for determining rainout and washout contributions of particulate elements and species shared in both particulate and dissolved phases.

415

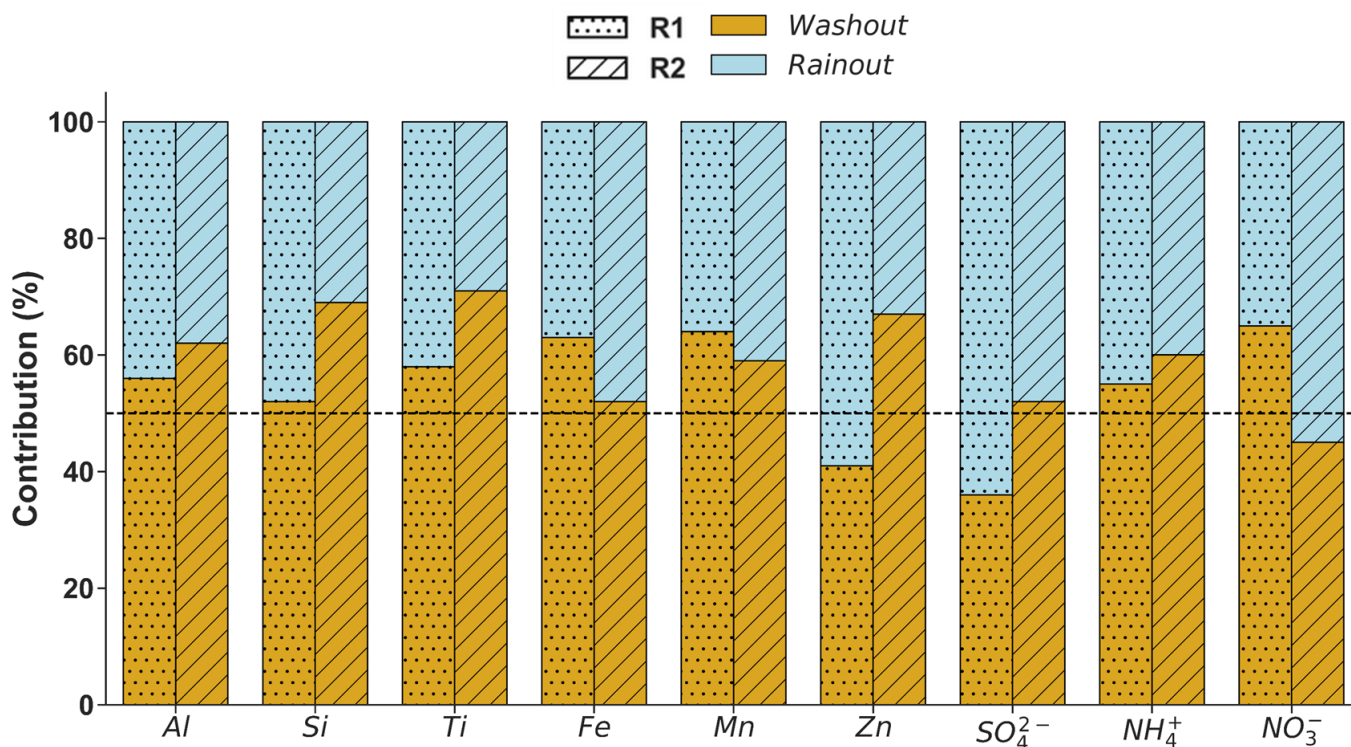
Chatterjee et al. (2010) as well as Karşı et al. (2018) have determined rainout and washout relative contributions on wet deposition of ionic species using sequential collection. On one hand, Chatterjee et al. (2010) defined two sub-events (named « below cloud » and « in-cloud » events) based on their respective evolution. The earlier stage of the precipitation where the concentrations decrease is higher being considered as below cloud event while the samples collected as the end of the rain event, where the decrease of concentrations shows a slower trend was considered as in-cloud event. On the other hand, Karşı et al. (2018) have used the average of at least the three lowest values as representative of the rainout droplet concentration, assumed to be representative of in-cloud concentrations prior any influence of washout. Then, rainout fluxes are compared to the total (rainout + washout) wet deposition fluxes to determine its relative contribution to wet deposition. Based on their approach, we determine in-cloud concentrations,  $C_{rainout}$  ( $\mu\text{g L}^{-1}$ ), for SNA, Fe, Si, Al, Ti, Zn and Mn using the VWM concentration of the constant level reached at the end of the rainfall for R1 (1.48 – 2.65 mm) and R2 (1.02 – 1.33 mm for SNA and 0.89 – 1.33 mm for other elements).

Values found for sulfate are similar for both events, between 259 and 287  $\mu\text{g L}^{-1}$ , which is lower than in-cloud concentrations previously observed using sequential sampling in an urban environment in Japan and China (1 880 - 3 330  $\mu\text{g L}^{-1}$ ; Aikawa et al., 2014; Xu et al., 2017; Ge et al., 2021). This is consistent with higher levels of SO<sub>2</sub> emissions in Asia than in Europe (e.g., Zhong et al., 2020). Concerning nitrate and ammonium, we found in-cloud concentrations ~2.4 times higher for R2 (1 147  $\mu\text{g L}^{-1}$  and 645  $\mu\text{g L}^{-1}$ , respectively) than for R1. These values are lower than values previously observed in urban environment in China (2 320 – 2 750  $\mu\text{g L}^{-1}$  and 1 390 – 2 510  $\mu\text{g L}^{-1}$  for nitrate and ammonium, respectively; Xu et al., 2017; Ge et al., 2021). However, nitrate in-cloud concentrations are higher than an urban environment in Austria (240  $\mu\text{g L}^{-1}$ ) (Monteiro et al., 2021). This illustrates therefore the various regional influences that can be observed in different urban environments.

435

The first fractions of rainfall are influenced by both washout and rainout processes. It is therefore necessary to subtract rainout influence at the beginning of the event in order to determine their relative contributions to total wet deposition. To do so, once  $C_{rainout}$  is obtained, we calculate the wet deposition fluxes due to the rainout process ( $F_{rainout} (\mu\text{g m}^{-2}) = C_{rainout} \times P_{tot}$ ) according to what has been previously done in the literature (e.g., Aikawa and Hiraki, 2009; Ge et al., 2016; Xu et al., 2017),  $P_{tot}$  being the rainfall depth of the event, and subtract it to the accumulated wet deposition flux ( $F_{wet\_dep}$ ,  $\mu\text{g m}^{-2}$ ).

We thus used the ratio  $\frac{F_{rainout}}{F_{wet\_dep}}$  (%) to estimate the wet deposition due to rainout process of Al, Si, Fe, Ti, Mn, Zn, SO<sub>4</sub><sup>2-</sup>, NH<sub>4</sub><sup>+</sup> and NO<sub>3</sub><sup>-</sup> for R1 and R2 (Figure 9).



445

**Figure 9. Rainout (light blue) and washout (orange) relative contribution for chemical species for R1 (dotted) and R2 (cross hatched). The dotted line corresponds to a relative contribution of 50%.**

We observe variations in washout and rainout relative contributions of studied chemical species within each rain (Fig. 9). The washout process is predominant for Al and Si, which are present in the coarse fraction, yet it is more marked for R2 (62 – 450 69%) than R1 (52 – 57%). We observe as well the same behavior for smaller particles such as Ti (58 and 72% for R1 and R2, respectively). These elements are of crustal origin and the dominant washout contribution is similar to what has been observed for Ca in different environments (66 – 99%; Ge et al., 2016; Berberler et al., 2022). Fe and Mn are mainly scavenged by washout as well but, they have also anthropogenic sources. Indeed, enrichment factors (EF, Taylor and McLennan, 1985)

relative to the Earth's crust were calculated using their total concentrations as follows:  $EF = \frac{([X]/[Al])_{\text{sample}}}{([X]/[Al])_{\text{crust}}}$ , where  $[X]/[Al]$  is

455 the ratio between the concentrations of an element X and Si in rainwater samples and in the upper continental crust. Fe is characterized by EF of 2 and 6 while Mn exhibits higher EF of 4 and 9, for R1 and R2, respectively. Washout contributions of Fe (62 vs. 52%) and Mn (64 vs. 59%) are more important for R1 than R2. Zn is an element with a well-marked anthropogenic source with EF of 226 and 396 for R1 and R2, respectively. Additional local emission of Zn in winter such as residential heating (oil and wood heating system; Citepa, 2022) can explain a higher washout relative contribution for R2 (67%) than R1 460 (41%). The same behavior is observed for SO<sub>4</sub><sup>2-</sup>, with a washout relative contribution of sulfate higher for R2 (52%) than R1 (38%) that can also be attributed to residential heating, explaining higher local emissions of SO<sub>2</sub> in the region in winter (oil

and wood heating system; Airparif, 2021; Favez et al., 2021). Ammonium is mainly deposited by washout for both events (55 – 60%). For nitrate, washout relative contribution is higher for R1 than R2 (65 vs. 45%) and could be due to a difference of the main nitrate form depending on the season (gaseous in summer vs. particulate in winter). Nevertheless, these chemical species are also influenced by the presence of the gaseous phase ( $\text{SO}_2$ ,  $\text{NO}_x$  and  $\text{NH}_3$ ) which make the comparison with other particulate elements sensitive. Relative contributions of washout and rainout also differ in the literature. For example, the relative contribution of rainout for sulfate shows a large variability in the literature in studies for urban environment (e.g., 12% in China, Ge et al. 2016; 84% in Japan, Aikawa et al. 2014). Nitrates rainout contribution values found in the literature also exhibits a high level of variability for urban environments in China (39 – 41%, Xu et al., 2017), in Turkey (10 – 40%, Karşı et al., 2018; 2.2 – 31%, Berberler et al., 2022) and for urban and suburban environments in Japan (26 – 40%, Aikawa et al., 2014; Aikawa and Hiraki, 2009). Therefore, new observations performed in our study contributes to the documentation and quantification of large variability within a rain event.

Our results show that Al, Ti, Mn and  $\text{NH}_4^+$  are in majority deposited via washout processes (57 – 62%, 52 – 69%, 58 – 72%, 59 – 64% and 55 – 60%, respectively) for both R1 and R2 events (Fig. 9). However, the predominance of rainout to total wet deposition depends on the rain event for Zn,  $\text{NO}_3^-$  and  $\text{SO}_4^{2-}$  (33 – 59%, 35 – 55% and 48 – 62%, respectively) for both rain events. In contrast, washout processes are predominant during R1 for Fe (64%) and R2 for Si (69%) while wet deposition is approximately due to rainout (48%) and washout (52%) processes equally during R2 for Fe and R1 for Si. Therefore, our study shows a more pronounced local contribution of  $\text{NH}_4^+$ , Al, Ti and Mn for both rain events, while the contribution of the local and medium to long-range of other species in wet deposition (Zn, Fe, Si,  $\text{NO}_3^-$  and  $\text{SO}_4^{2-}$ ) differs according to the event.

#### 4. Conclusion

The sequential sampler developed in this study allows investigating the time evolution of chemical composition of wet deposition throughout a rainfall event, down to trace levels. It has a large collection area and an automatic distribution system ensuring a high temporal resolution to analyze both dissolved and particulate phases as well as major and trace species in elemental and ionic compositions of rainfall.

The chemical compositions of rainfall are consistent with the specificity of air quality in Paris and its region. The dominant dissolved species are inorganic ions (SNA: sulfate, nitrate and ammonium). It is interesting to note that Al, Fe, Si and Ti are overwhelmingly present in the particulate phase of rain, even in this urban environment, while Trace Metals (TMs) such as Mn and Zn are present in both the dissolved and particulate phases. For these elements, we observed an increasing dissolved/total ratio as the rainfall progress. This intra-event evolution probably involves the effect of dissolution time into rain droplets (in relation with washout or rainout scavenging) and the evolution of the nature of scavenged particles. The time resolution of rainfall composition allows determining washout and rainout relative contribution to total wet deposition for

SNA, some insoluble elements (Si, Al, Fe and Ti) as well as TMs for both events. Our results show that Al, Fe, Si, Ti, Mn and  
495  $\text{NH}_4^+$  are in majority deposited via washout processes while the predominance of rainout or washout processes to the wet  
deposition of Zn,  $\text{NO}_3^-$  and  $\text{SO}_4^{2-}$  depends on the rain event.

The sequential sampling allows us to study the link between deposition fluxes and rainfall pattern. The total mass  
concentrations of rain sharply decrease in the beginning of rainfall so that around 15% of the total mass of wet deposition  
fluxes is deposited within the first 4% of rainfall depth, whatever the intensity pattern of rainfall. Mass concentrations  
500 throughout rainfall events are not only dependent on rainfall depth, but also to the variation of the rainfall rate regime within  
the rain event. Indeed, we observed for both rain events an increasing sulfate, nitrates and ammonium concentrations in the  
dissolved phase correlated with rainfall rates decrease and with an increase of the relative weight of smaller droplets. This  
increase may result from either an increase in the scavenging efficiency or from an increase in droplet evaporation during their  
fall.

505

In order to link the evolution of dissolved to total ratio with these scavenging processes, concomitant measurements on  
atmospheric aerosols (e.g., homogeneity of the air column, aerosol chemical content and particle size distribution) and  
meteorological parameters (e.g., cloud base height, droplet size distribution and rainfall rate) during the rain sampling need to  
be planned in future experiments.

## 510 **Acknowledgments**

This work is performed in the framework of the research programs DATSHA supported by the French national program LEFE  
(Les Enveloppes Fluides et Environnement) and Foundation Air Liquide, and was also supported by LISA UPC, UPEC, UMR  
CNRS 7583 via its internal project call. The analyses presented were performed with the instruments of the PRAMMICS  
platform OSU-EFLUVE UMS 3563. **The authors would like to acknowledge SIRTA for providing the ceilometer data**  
515 **used in this study.**

## **References**

- Aikawa, M. and Hiraki, T.: Washout/rainout contribution in wet deposition estimated by 0.5 mm precipitation  
sampling/analysis, *Atmospheric Environment*, 43, 4935–4939, <https://doi.org/10.1016/j.atmosenv.2009.07.057>, 2009.
- Aikawa, M., Kajino, M., Hiraki, T., and Mukai, H.: The contribution of site to washout and rainout: Precipitation chemistry  
520 based on sample analysis from 0.5 mm precipitation increments and numerical simulation, *Atmospheric Environment*, 95,  
165–174, <https://doi.org/10.1016/j.atmosenv.2014.06.015>, 2014.
- Airparif: Synthèse des connaissances sur les particules en Île-de-France, 2021.

- Ambe, Y. and Nishikawa, M.: Temporal variation of trace element concentrations in selected rainfall events at Tsukuba, Japan, *Atmospheric Environment* (1967), 20, 1931–1940, [https://doi.org/10.1016/0004-6981\(86\)90334-3](https://doi.org/10.1016/0004-6981(86)90334-3), 1986a.
- 525 Ambe, Y. and Nishikawa, M.: Variations in different sized water insoluble particulate matter in rain water, *Atmospheric Environment* (1967), 21, 1469–1471, [https://doi.org/10.1016/0004-6981\(67\)90095-9](https://doi.org/10.1016/0004-6981(67)90095-9), 1986b.
- Ames, D. L., Roberts, L. E., and Webb, A. H.: An automatic rain gauge for continuous, real time determination of rainwater chemistry, *Atmospheric Environment* (1967), 21, 1947–1955, [https://doi.org/10.1016/0004-6981\(87\)90155-7](https://doi.org/10.1016/0004-6981(87)90155-7), 1987.
- 530 Anil, I., Alagha, O., and Karaca, F.: Effects of transport patterns on chemical composition of sequential rain samples: trajectory clustering and principal component analysis approach, *Air Quality, Atmosphere & Health*, 10, 1193–1206, <https://doi.org/10.1007/s11869-017-0504-x>, 2017.
- Asman, W. A. H.: Draft, construction and operation of a sequential rain sampler, *Water, Air, and Soil Pollution*, 13, 235–245, <https://doi.org/10.1007/BF02279550>, 1980.
- 535 Baechmann, K., Ebert, P., Haag, I., and Prokop, T.: The chemical content of raindrops as a function of drop radius—I. Field measurements at the cloud base and below the cloud, *Atmospheric Environment*, 30, 1019–1025, [https://doi.org/10.1016/1352-2310\(95\)00409-2](https://doi.org/10.1016/1352-2310(95)00409-2), 1996a.
- Baechmann, K., Ebert, P., Haag, I., Prokop, T., and Steigerwald, K.: The chemical content of raindrops as a function of drop radius—II. Field experimental study on the scavenging of marked aerosol particles by raindrops sampled as a function of drop size, *Atmospheric Environment*, 30, 1027–1033, [https://doi.org/10.1016/1352-2310\(95\)00325-8](https://doi.org/10.1016/1352-2310(95)00325-8), 1996b.
- 540 Báez, A. P., Belmont, R., and G, H. P.: Variation of chemical composition of wet precipitation, using a sequential sampling: urban-rural areas comparison, *Atmósfera*, 6, 163–174, 1993.
- Berberler, E., Gemici, B. T., Uzun Özel, H., Demir, T., and Karakaş, D.: Source identification of water-insoluble single particulate matters in rain sequences, *Atmospheric Pollution Research*, 13, 101499, <https://doi.org/10.1016/j.apr.2022.101499>, 2022.
- 545 Bergametti, G., Gomes, L., Remoudaki, E., Desbois, M., Martin, D., and Buat-Ménard, P.: Present Transport and Deposition Patterns of African Dusts to the North-Western Mediterranean, in: *Paleoclimatology and Paleometeorology: Modern and Past Patterns of Global Atmospheric Transport*, edited by: Leinen, M. and Sarnthein, M., Springer Netherlands, Dordrecht, 227–252, [https://doi.org/10.1007/978-94-009-0995-3\\_9](https://doi.org/10.1007/978-94-009-0995-3_9), 1989.
- 550 Bertrand, G., Celle-Jeanton, H., Laj, P., Rangognio, J., and Chazot, G.: Rainfall chemistry: long range transport versus below cloud scavenging. A two-year study at an inland station (Opme, France), *Journal of Atmospheric Chemistry*, 60, 253–271, <https://doi.org/10.1007/s10874-009-9120-y>, 2008.
- Beysens, D., Mongruel, A., and Acker, K.: Urban dew and rain in Paris, France: Occurrence and physico-chemical characteristics, *Atmospheric Research*, 189, 152–161, <https://doi.org/10.1016/j.atmosres.2017.01.013>, 2017.
- 555 Bukowiecki, N., Lienemann, P., Hill, M., Figi, R., Richard, A., Furger, M., Rickers, K., Falkenberg, G., Zhao, Y., and Cliff, S. S.: Real-world emission factors for antimony and other brake wear related trace elements: size-segregated values for light and heavy duty vehicles, *Environmental Science & Technology*, 43, 8072–8078, 2009.
- Burch, H., Waldner, P., and Fritschi, B.: Variation of pH and concentration of nutrients and minerals during rain-events, in: *Ecological processes in small basins: Sixth Conference of the European Network of Experimental and Representative Basins (ERB)*, Strasbourg, France, 59–64, 1996.

- 560 Calvo, A. I., Pont, V., Olmo, F. J., Castro, A., Alados-Arboledas, L., Vicente, A. M., Fernández-Raga, M., and Fraile, R.: Air Masses and Weather Types: A Useful Tool for Characterizing Precipitation Chemistry and Wet Deposition, *Aerosol and Air Quality Research*, 12, 856–878, <https://doi.org/10.4209/aaqr.2012.03.0068>, 2012.
- Cao, Y.-Z., Wang, S., Zhang, G., Luo, J., and Lu, S.: Chemical characteristics of wet precipitation at an urban site of Guangzhou, South China, *Atmospheric Research*, 94, 462–469, <https://doi.org/10.1016/j.atmosres.2009.07.004>, 2009.
- 565 Cao, Z., Zhou, X., Ma, Y., Wang, L., Wu, R., Chen, B., and Wang, W.: The Concentrations, Formations, Relationships and Modeling of Sulfate, Nitrate and Ammonium (SNA) Aerosols over China, *Aerosol and Air Quality Research*, 17, 84–97, <https://doi.org/10.4209/aaqr.2016.01.0020>, 2017.
- Castillo, S., Alastuey, A., Cuevas, E., Querol, X., and Avila, A.: Quantifying Dry and Wet Deposition Fluxes in Two Regions of Contrasting African Influence: The NE Iberian Peninsula and the Canary Islands, *Atmosphere*, 8, 86,  
570 <https://doi.org/10.3390/atmos8050086>, 2017.
- Celle-Jeanton, H., Travi, Y., Loÿe-Pilot, M.-D., Huneau, F., and Bertrand, G.: Rainwater chemistry at a Mediterranean inland station (Avignon, France): Local contribution versus long-range supply, *Atmospheric Research*, 91, 118–126, <https://doi.org/10.1016/j.atmosres.2008.06.003>, 2009.
- Chatterjee, A., Jayaraman, A., Rao, T. N., and Raha, S.: In-cloud and below-cloud scavenging of aerosol ionic species over a  
575 tropical rural atmosphere in India, *Journal of Atmospheric Chemistry*, 66, 27–40, <https://doi.org/10.1007/s10874-011-9190-5>, 2010.
- Chelin, P., Viatte, C., Ray, M., Eremenko, M., Cuesta, J., Hase, F., Orphal, J., and Flaud, J.-M.: The OASIS Observatory Using Ground-Based Solar Absorption Fourier-Transform Infrared Spectroscopy in the Suburbs of Paris (Créteil-France), in: *Environment, Energy and Climate Change I: Environmental Chemistry of Pollutants and Wastes*, edited by: Jiménez, E.,  
580 Cabañas, B., and Lefebvre, G., Springer International Publishing, Cham, 21–52, [https://doi.org/10.1007/698\\_2014\\_270](https://doi.org/10.1007/698_2014_270), 2015.
- Cheng, I., Al Mamun, A., and Zhang, L.: A synthesis review on atmospheric wet deposition of particulate elements: scavenging ratios, solubility, and flux measurements, *Environmental Reviews*, 29, 340–353, <https://doi.org/10.1139/er-2020-0118>, 2021.
- Citepa: Inventaire des émissions de polluants atmosphériques et de gaz à effet de serre en France - Format Secten, CITEPA, 2022.
- 585 Croft, B., Lohmann, U., Martin, R. V., Stier, P., Wurzler, S., Feichter, J., Hoose, C., Heikkilä, U., van Donkelaar, A., and Ferrachat, S.: Influences of in-cloud aerosol scavenging parameterizations on aerosol concentrations and wet deposition in ECHAM5-HAM, *Atmospheric Chemistry and Physics*, 10, 1511–1543, <https://doi.org/10.5194/acp-10-1511-2010>, 2010.
- Desboeufs, K., Journet, E., Rajot, J.-L., Chevaillier, S., Triquet, S., Formenti, P., and Zakou, A.: Chemistry of rain events in West Africa: evidence of dust and biogenic influence in convective systems, *Atmospheric Chemistry and Physics*, 10, 9283–  
590 9293, <https://doi.org/10.5194/acp-10-9283-2010>, 2010.
- Desboeufs, K., Fu, F., Bressac, M., Tovar-Sánchez, A., Triquet, S., Doussin, J.-F., Giorio, C., Chazette, P., Disnaquet, J., Feron, A., Formenti, P., Maisonneuve, F., Rodríguez-Romero, A., Zapf, P., Dulac, F., and Guieu, C.: Wet deposition in the remote western and central Mediterranean as a source of trace metals to surface seawater, *Atmospheric Chemistry and Physics*, 22, 2309–2332, <https://doi.org/10.5194/acp-22-2309-2022>, 2022.
- 595 Draxler, R. R. and Rolph, G. D.: HYSPLIT (HYbrid Single-Particle Lagrangian Integrated Trajectory) Model access via NOAA ARL READY Website, <http://ready.arl.noaa.gov/HYSPLIT.php>, 2012.

- 600 Duce, R. A., Liss, P. S., Merrill, J. T., Atlas, E. L., Buat-Menard, P., Hicks, B. B., Miller, J. M., Prospero, J. M., Arimoto, R., Church, T. M., Ellis, W., Galloway, J. N., Hansen, L., Jickells, T. D., Knap, A. H., Reinhardt, K. H., Schneider, B., Soudine, A., Tokos, J. J., Tsunogai, S., Wollast, R., and Zhou, M.: The atmospheric input of trace species to the world ocean, *Global Biogeochemical Cycles*, 5, 193–259, <https://doi.org/10.1029/91GB01778>, 1991.
- Fan, S.-M., Moxim, W. J., and Levy II, H.: Aeolian input of bioavailable iron to the ocean, *Geophysical Research Letters*, 33, <https://doi.org/10.1029/2005GL024852>, 2006.
- 605 Favez, O., Weber, S., Petit, J.-E., Alleman, L. Y., Albinet, A., Riffault, V., Chazeau, B., Amodeo, T., Salameh, D., Zhang, Y., Srivastava, D., Samaké, A., Aujay-Plouzeau, R., Papin, A., Bonnaire, N., Boullanger, C., Chatain, M., Chevrier, F., Detournay, A., Dominik-Sègue, M., Falhun, R., Garbin, C., Gherzi, V., Grignion, G., Levigoureux, G., Pontet, S., Rangognio, J., Zhang, S., Besombes, J.-L., Conil, S., Uzu, G., Savarino, J., Marchand, N., Gros, V., Marchand, C., Jaffrezo, J.-L., and Leoz-Garziandia, E.: Overview of the French Operational Network for In Situ Observation of PM Chemical Composition and Sources in Urban Environments (CARA Program), *Atmosphere*, 12, 207, <https://doi.org/10.3390/atmos12020207>, 2021.
- 610 Galloway, J. N., Townsend, A. R., Erisman, J. W., Bekunda, M., Cai, Z., Freney, J. R., Martinelli, L. A., Seitzinger, S. P., and Sutton, M. A.: Transformation of the Nitrogen Cycle: Recent Trends, Questions, and Potential Solutions, *Science*, 320, 889–892, <https://doi.org/10.1126/science.1136674>, 2008.
- Ge, B., Wang, Z., Gbaguidi, A. E., and Zhang, Q.: Source Identification of Acid Rain Arising over Northeast China: Observed Evidence and Model Simulation, *Aerosol and Air Quality Research*, 16, 1366–1377, <https://doi.org/10.4209/aaqr.2015.05.0294>, 2016.
- 615 Ge, B., Xu, D., Wild, O., Yao, X., Wang, J., Chen, X., Tan, Q., Pan, X., and Wang, Z.: Inter-annual variations of wet deposition in Beijing from 2014–2017: implications of below-cloud scavenging of inorganic aerosols, *Atmospheric Chemistry and Physics*, 21, 9441–9454, <https://doi.org/10.5194/acp-21-9441-2021>, 2021.
- 620 Germer, S., Neill, C., Krusche, A. V., Neto, S. C. G., and Elsenbeer, H.: Seasonal and within-event dynamics of rainfall and throughfall chemistry in an open tropical rainforest in Rondônia, Brazil, *Biogeochemistry*, 86, 155–174, <https://doi.org/10.1007/s10533-007-9152-9>, 2007.
- Gong, W., Stroud, C., and Zhang, L.: Cloud Processing of Gases and Aerosols in Air Quality Modeling, *Atmosphere*, 2, 567–616, <https://doi.org/10.3390/atmos2040567>, 2011.
- 625 González, C. M. and Aristizábal, B. H.: Acid rain and particulate matter dynamics in a mid-sized Andean city: The effect of rain intensity on ion scavenging, *Atmospheric Environment*, 60, 164–171, <https://doi.org/10.1016/j.atmosenv.2012.05.054>, 2012.
- Greenfield, S. M.: Rain scavenging of radioactive particulate matter from the atmosphere, *Journal of Meteorology*, 14, 115–125, [https://doi.org/10.1175/1520-0469\(1957\)014<0115:RSORPM>2.0.CO;2](https://doi.org/10.1175/1520-0469(1957)014<0115:RSORPM>2.0.CO;2), 1957.
- 630 Haeffelin, M., Barthès, L., Bock, O., Boitel, C., Bony, S., Bouniol, D., Chepfer, H., Chiriaco, M., Cuesta, J., Delanoë, J., Drobinski, P., Dufresne, J.-L., Flamant, C., Grall, M., Hodzic, A., Hourdin, F., Lapouge, F., Lemaître, Y., Mathieu, A., Morille, Y., Naud, C., Noël, V., O’Hirok, W., Pelon, J., Pietras, C., Protat, A., Romand, B., Scialom, G., and Vautard, R.: SIRTa, a ground-based atmospheric observatory for cloud and aerosol research, *Annales Geophysicae*, 23, 253–275, <https://doi.org/10.5194/angeo-23-253-2005>, 2005.
- 635 Hicks, B. B. and Shannon, J. D.: A Method for Modeling the Deposition of Sulfur by Precipitation over Regional Scales, *Journal of Applied Meteorology and Climatology*, 18, 1415–1420, [https://doi.org/10.1175/1520-0450\(1979\)018<1415:AMFMTD>2.0.CO;2](https://doi.org/10.1175/1520-0450(1979)018<1415:AMFMTD>2.0.CO;2), 1979.

- Huff, F. A. and Stout, G. E.: Distribution of Radioactive Rainout in Convective Rainfall, *Journal of Applied Meteorology* (1962-1982), 3, 707–717, 1964.
- Jaffrezo, J.-L. and Colin, J.-L.: Rain-aerosol coupling in urban area: Scavenging ratio measurement and identification of some transfer processes, *Atmospheric Environment* (1967), 22, 929–935, [https://doi.org/10.1016/0004-6981\(88\)90270-3](https://doi.org/10.1016/0004-6981(88)90270-3), 1988.
- 640 Jickells, T. D., Baker, A. R., and Chance, R.: Atmospheric transport of trace elements and nutrients to the oceans, *Philosophical Transactions of the Royal Society A: Mathematical, Physical and Engineering Sciences*, 374, 20150286, <https://doi.org/10.1098/rsta.2015.0286>, 2016.
- Jordi, A., Basterretxea, G., Tovar-Sánchez, A., Alastuey, A., and Querol, X.: Copper aerosols inhibit phytoplankton growth in the Mediterranean Sea, *Proceedings of the National Academy of Sciences*, 109, 21246–21249, 645 <https://doi.org/10.1073/pnas.1207567110>, 2012.
- Karşı, M. B. B., Yenisoy-Karakaş, S., and Karakaş, D.: Investigation of washout and rainout processes in sequential rain samples, *Atmospheric Environment*, 190, 53–64, <https://doi.org/10.1016/j.atmosenv.2018.07.018>, 2018.
- Kasahara, M., Ogiwara, H., and Yamamoto, K.: Soluble and insoluble components of air pollutants scavenged by rain water, *Nuclear Instruments and Methods in Physics Research Section B: Beam Interactions with Materials and Atoms*, 118, 400–402, 650 [https://doi.org/10.1016/0168-583X\(95\)01087-4](https://doi.org/10.1016/0168-583X(95)01087-4), 1996.
- Keene, W. C., Pszenny, A. A. P., Galloway, J. N., and Hawley, M. E.: Sea-salt corrections and interpretation of constituent ratios in marine precipitation, *Journal of Geophysical Research: Atmospheres*, 91, 6647–6658, <https://doi.org/10.1029/JD091iD06p06647>, 1986.
- Keene, W. C., Galloway, J. N., Likens, G. E., Deviney, F. A., Mikkelsen, K. N., Moody, J. L., and Maben, J. R.: Atmospheric 655 Wet Deposition in Remote Regions: Benchmarks for Environmental Change, *Journal of the Atmospheric Sciences*, 72, 2947–2978, <https://doi.org/10.1175/JAS-D-14-0378.1>, 2015.
- Keresztesi, Á., Birsan, M.-V., Nita, I.-A., Bodor, Z., and Szép, R.: Assessing the neutralisation, wet deposition and source contributions of the precipitation chemistry over Europe during 2000–2017, *Environmental Sciences Europe*, 31, 50, <https://doi.org/10.1186/s12302-019-0234-9>, 2019.
- 660 Krupa, S. V.: Sampling and physico-chemical analysis of precipitation: a review, *Environmental Pollution*, 120, 565–594, [https://doi.org/10.1016/S0269-7491\(02\)00165-3](https://doi.org/10.1016/S0269-7491(02)00165-3), 2002.
- Kulshrestha, U. C., Reddy, L. A. K., Satyanarayana, J., and Kulshrestha, M. J.: Real-time wet scavenging of major chemical constituents of aerosols and role of rain intensity in Indian region, *Atmospheric Environment*, 43, 5123–5127, <https://doi.org/10.1016/j.atmosenv.2009.07.025>, 2009.
- 665 Laquer, F. C.: Sequential precipitation samplers: A literature review, *Atmospheric Environment. Part A. General Topics*, 24, 2289–2297, [https://doi.org/10.1016/0960-1686\(90\)90322-E](https://doi.org/10.1016/0960-1686(90)90322-E), 1990.
- Lim, B., Jickells, T. D., and Davies, T. D.: Sequential sampling of particles, major ions and total trace metals in wet deposition, *Atmospheric Environment. Part A. General Topics*, 25, 745–762, [https://doi.org/10.1016/0960-1686\(91\)90073-G](https://doi.org/10.1016/0960-1686(91)90073-G), 1991.
- 670 Lindberg, S. E.: Factors influencing trace metal, sulfate and hydrogen ion concentrations in rain, *Atmospheric Environment* (1967), 16, 1701–1709, [https://doi.org/10.1016/0004-6981\(82\)90263-3](https://doi.org/10.1016/0004-6981(82)90263-3), 1982.

- Luo, W.: Wet-deposition fluxes of soluble chemical species and the elements in insoluble materials, *Atmospheric Environment*, 35, 2963–2967, [https://doi.org/10.1016/S1352-2310\(00\)00484-2](https://doi.org/10.1016/S1352-2310(00)00484-2), 2001.
- Ma, C.-J.: Chemical composition of a yellowish rainfall by the application of PIXE and micro-PIXE technique, *Nuclear Instruments and Methods in Physics Research Section B: Beam Interactions with Materials and Atoms*, 251, 501–506, <https://doi.org/10.1016/j.nimb.2006.07.025>, 2006.
- 675 Mackey, K., Buck, K., Casey, J., Cid, A., Lomas, M., Sohrin, Y., and Paytan, A.: Phytoplankton responses to atmospheric metal deposition in the coastal and open-ocean Sargasso Sea, *Frontiers in Microbiology*, 3, 2012.
- Mamun, A. A., Cheng, I., Zhang, L., Dabek-Zlotorzynska, E., and Charland, J.-P.: Overview of size distribution, concentration, and dry deposition of airborne particulate elements measured worldwide, *Environmental Reviews*, 28, 77–88, 2020.
- 680 Method 1638: Determination of trace elements in ambient waters by inductively coupled plasma-mass spectrometry, US Environmental Protection Agency Washington, DC, 1996.
- Monteiro, L. R., Terzer-Wassmuth, S., Matiatos, I., Douence, C., and Wassenaar, L. I.: Distinguishing in-cloud and below-cloud short and distal N-sources from high-temporal resolution seasonal nitrate and ammonium deposition in Vienna, Austria, *Atmospheric Environment*, 266, 118740, <https://doi.org/10.1016/j.atmosenv.2021.118740>, 2021.
- 685 Pant, P. and Harrison, R. M.: Estimation of the contribution of road traffic emissions to particulate matter concentrations from field measurements: A review, *Atmospheric Environment*, 77, 78–97, <https://doi.org/10.1016/j.atmosenv.2013.04.028>, 2013.
- Paytan, A., Mackey, K. R. M., Chen, Y., Lima, I. D., Doney, S. C., Mahowald, N., Labiosa, R., and Post, A. F.: Toxicity of atmospheric aerosols on marine phytoplankton, *Proceedings of the National Academy of Sciences*, 106, 4601–4605, <https://doi.org/10.1073/pnas.0811486106>, 2009.
- 690 Pruppacher, H. R. and Klett, J. D.: *Microphysics of Clouds and Precipitation*, Springer Science & Business Media, 988 pp., 1996.
- Richon, C., Dutay, J.-C., Dulac, F., Wang, R., and Balkanski, Y.: Modeling the biogeochemical impact of atmospheric phosphate deposition from desert dust and combustion sources to the Mediterranean Sea, *Biogeosciences*, 15, 2499–2524, <https://doi.org/10.5194/bg-15-2499-2018>, 2018.
- 695 Ryu, Y.-H. and Min, S.-K.: Improving Wet and Dry Deposition of Aerosols in WRF-Chem: Updates to Below-Cloud Scavenging and Coarse-Particle Dry Deposition, *Journal of Advances in Modeling Earth Systems*, 14, e2021MS002792, <https://doi.org/10.1029/2021MS002792>, 2022.
- Safai, P. D., Rao, P. S. P., Momin, G. A., Ali, K., Chate, D. M., and Praveen, P. S.: Chemical composition of precipitation during 1984–2002 at Pune, India, *Atmospheric Environment*, 38, 1705–1714, <https://doi.org/10.1016/j.atmosenv.2003.12.016>, 2004.
- 700 Sanderson, P., Delgado-Saborit, J. M., and Harrison, R. M.: A review of chemical and physical characterisation of atmospheric metallic nanoparticles, *Atmospheric Environment*, 94, 353–365, <https://doi.org/10.1016/j.atmosenv.2014.05.023>, 2014.
- Schaap, M., van Loon, M., ten Brink, H. M., Dentener, F. J., and Builtjes, P. J. H.: Secondary inorganic aerosol simulations for Europe with special attention to nitrate, *Atmospheric Chemistry and Physics*, 4, 857–874, <https://doi.org/10.5194/acp-4-857-2004>, 2004.
- 705

- Seinfeld, J. H. and Pandis, S. N.: Atmospheric Chemistry and Physics: From Air Pollution to Climate Change, John Wiley & Sons, 1146 pp., 2016.
- Seymour, M. D., Schubert, S. A., Wesley Clayton, J., and Fernando, Q.: Variations in the acid content of rain water in the course of a single precipitation, *Water, Air, and Soil Pollution*, 10, 147–161, <https://doi.org/10.1007/BF00464711>, 1978.
- 710 Shimamura, T., Wada, T., Iwashita, M., Takaku, Y., and Ohashi, H.: Scavenging properties of major and trace species in rainfall collected in urban and suburban Tokyo, *Atmospheric Environment*, 40, 4220–4227, <https://doi.org/10.1016/j.atmosenv.2006.03.010>, 2006.
- Slinn, W. G. N.: Some approximations for the wet and dry removal of particles and gases from the atmosphere, *Water, Air, and Soil Pollution*, 7, <https://doi.org/10.1007/BF00285550>, 1977.
- 715 Tang, A., Zhuang, G., Wang, Y., Yuan, H., and Sun, Y.: The chemistry of precipitation and its relation to aerosol in Beijing, *Atmospheric Environment*, 39, 3397–3406, <https://doi.org/10.1016/j.atmosenv.2005.02.001>, 2005.
- Taylor, S. R. and McLennan, S. M.: *The continental crust: Its composition and evolution*, 1985.
- Textor, C., Schulz, M., Guibert, S., Kinne, S., Balkanski, Y., Bauer, S., Berntsen, T., Berglen, T., Boucher, O., Chin, M., Dentener, F., Diehl, T., Easter, R., Feichter, H., Fillmore, D., Ghan, S., Ginoux, P., Gong, S., Grini, A., Hendricks, J., Horowitz, L., Huang, P., Isaksen, I., Iversen, T., Kloster, S., Koch, D., Kirkeva, A., Kristjansson, J. E., Krol, M., Lauer, A., Lamarque, J. F., Liu, X., Montanaro, V., Myhre, G., Penner, J., Pitari, G., Reddy, S., Seland, Ø., Stier, P., Takemura, T., and Tie, X.: Analysis and quantification of the diversities of aerosol life cycles within AeroCom, *Atmospheric Chemistry and Physics*, 37, <https://doi.org/10.5194/acp-6-1777-2006>, 2006.
- 720
- Thorpe, A. and Harrison, R. M.: Sources and properties of non-exhaust particulate matter from road traffic: A review, *Science of The Total Environment*, 400, 270–282, <https://doi.org/10.1016/j.scitotenv.2008.06.007>, 2008.
- 725
- Van Wambeke, F., Taillandier, V., Desboeufs, K., Pulido-Villena, E., Dinasquet, J., Engel, A., Marañón, E., Ridame, C., and Guieu, C.: Influence of atmospheric deposition on biogeochemical cycles in an oligotrophic ocean system, *Biogeosciences*, 18, 5699–5717, <https://doi.org/10.5194/bg-18-5699-2021>, 2021.
- Vet, R., Artz, R. S., Carou, S., Shaw, M., Ro, C.-U., Aas, W., Baker, A., Bowersox, V. C., Dentener, F., Galy-Lacaux, C., Hou, A., Pienaar, J. J., Gillett, R., Forti, M. C., Gromov, S., Hara, H., Khodzher, T., Mahowald, N. M., Nickovic, S., Rao, P. S. P., and Reid, N. W.: A global assessment of precipitation chemistry and deposition of sulfur, nitrogen, sea salt, base cations, organic acids, acidity and pH, and phosphorus, *Atmospheric Environment*, 93, 3–100, <https://doi.org/10.1016/j.atmosenv.2013.10.060>, 2014.
- 730
- Vincent, J., Laurent, B., Losno, R., Bon Nguyen, E., Roullet, P., Sauvage, S., Chevaillier, S., Coddeville, P., Ouboulmane, N., di Sarra, A. G., Tovar-Sánchez, A., Sferlazzo, D., Massanet, A., Triquet, S., Morales Baquero, R., Fournier, M., Coursier, C., Desboeufs, K., Dulac, F., and Bergametti, G.: Variability of mineral dust deposition in the western Mediterranean basin and south-east of France, *Atmospheric Chemistry and Physics*, 16, 8749–8766, <https://doi.org/10.5194/acp-16-8749-2016>, 2016.
- 735
- Wright, L. P., Zhang, L., Cheng, I., Aherne, J., and Wentworth, G. R.: Impacts and Effects Indicators of Atmospheric Deposition of Major Pollutants to Various Ecosystems - A Review, *Aerosol and Air Quality Research*, 18, 1953–1992, <https://doi.org/10.4209/aaqr.2018.03.0107>, 2018.
- 740
- Xu, D., Ge, B., Wang, Z., Sun, Y., Chen, Y., Ji, D., Yang, T., Ma, Z., Cheng, N., Hao, J., and Yao, X.: Below-cloud wet scavenging of soluble inorganic ions by rain in Beijing during the summer of 2014, *Environmental Pollution*, 230, 963–973, <https://doi.org/10.1016/j.envpol.2017.07.033>, 2017.

- 745 Yang, Q., Easter, R. C., Campuzano-Jost, P., Jimenez, J. L., Fast, J. D., Ghan, S. J., Wang, H., Berg, L. K., Barth, M. C., Liu, Y., Shrivastava, M. B., Singh, B., Morrison, H., Fan, J., Ziegler, C. L., Bela, M., Apel, E., Diskin, G. S., Mikoviny, T., and Wisthaler, A.: Aerosol transport and wet scavenging in deep convective clouds: A case study and model evaluation using a multiple passive tracer analysis approach, *Journal of Geophysical Research: Atmospheres*, 120, 8448–8468, <https://doi.org/10.1002/2015JD023647>, 2015.
- 750 Zhang, L. and Vet, R.: A review of current knowledge concerning size-dependent aerosol removal, *China Particuology*, 4, 272–282, [https://doi.org/10.1016/S1672-2515\(07\)60276-0](https://doi.org/10.1016/S1672-2515(07)60276-0), 2006.
- Zhao, T. L., Gong, S. L., Zhang, X. Y., and McKendry, I. G.: Modeled size-segregated wet and dry deposition budgets of soil dust aerosol during ACE-Asia 2001: Implications for trans-Pacific transport, *Journal of Geophysical Research: Atmospheres*, [https://doi.org/10.1029/2002JD003363@10.1002/\(ISSN\)2169-8996.ACEASIA1](https://doi.org/10.1029/2002JD003363@10.1002/(ISSN)2169-8996.ACEASIA1), 2003.
- 755 Zhong, Q., Shen, H., Yun, X., Chen, Y., Ren, Y., Xu, H., Shen, G., Du, W., Meng, J., Li, W., Ma, J., and Tao, S.: Global Sulfur Dioxide Emissions and the Driving Forces, *Environ. Sci. Technol.*, 54, 6508–6517, <https://doi.org/10.1021/acs.est.9b07696>, 2020.